Modelling of Grid connected Single Phase Two Stage Full Bridge Converter for Photovoltaic Application

by

Manish Patil

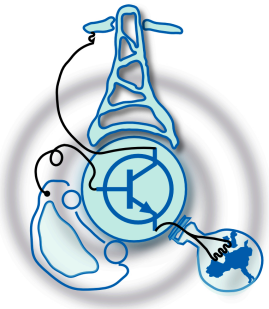

Submitted to the Department of Electrical Engineering, Electronics, Computers and Systems
in partial fulfillment of the requirements for the degree of
Master Course in Electrical Energy Conversion and Power Systems
at the
UNIVERSIDAD DE OVIEDO
July 2017

Author .....

Certified by .....
Jorge Garcia Garcia
Associate Professor
Thesis Supervisor

Certified by .....
Cristina Gonzalez Moran
Associate Professor
Thesis Supervisor

Modelling of Grid connected Single Phase Two Stage Full Bridge Converter for Photovoltaic Application

by

Manish Patil

Submitted to the Department of Electrical Engineering, Electronics, Computers and Systems
on July 21, 2017, in partial fulfillment of the
requirements for the degree of
Master Course in Electrical Energy Conversion and Power Systems

Abstract

This Master thesis presents modelling of Single phase two stage grid connected full bridge inverter. The whole system includes the PV modules, a boost converter and a full bridge Inverter. Reference datasheet of Monocristalline Silicon SLK72M6L have been used for the photovoltaic array. PV modules were made up of a number of PV cells connected in series and parallel.

One array consists of six PV panel. Then two arrays are connected in parallel. These PV arrays are used for generating electricity in PV generation systems. Thereafter, PV array have been simulated under varying environmental condition like varying irradiance, temperature and partial shading conditions. PV array evaluated by varying number of series, parallel array and by physical parameters like Rsh (shunt) and Rse (series) resistance. I-V and P-V operating curves studied closely under open loop of PV array. Observed open circuit current and voltage are around 9.02 A and 44.5 V respectively.

In the second part, circuit have been designed such that it delivers constant and step up DC voltage to load. Open loop boost converter has been studied by using constant DC voltage source and observed output voltage and current for boost converter. Thereafter, our study have been progressed by coupling PV array with boost converter. The characteristics of I-V and P-V curves of photovoltaic module coupled with boost converter were tuned by means of simulations to achieve Maximum Power Point (MPP) with optimal voltage and current Vmpp and Impp respectively. To achieve MPP, MPPT algorithm has been used.

In this system, output voltage of boost converter have been observed around 400 V to charge the DC link. In third model, full bridge inverter have been simulated in open loop to achieve required power at load. LCL filter has been designed at load side and achieved maximum power transfer. When power at input and output were made almost equal, load has been replaced with grid. Simulated open loop model has been replaced with closed loop model. Grid angle for phase lock loop have been used for alpha beta and D Q conversion. Finally it has been verified. By means of

step by step simulation, power loss for grid connected two stage full bridge inverter have been calculated. Finally full bridge inverter has been designed with parameter almost similar to Ingecon@Sunlite 5TL model (transformer less).

Thesis Supervisor: Jorge Garcia Garcia
Title: Associate Professor

Thesis Supervisor: Cristina Gonzalez Moran
Title: Associate Professor

Acknowledgments

I wish to express my sincere appreciation to all the people who helped me in many ways throughout my Master candidature at University of Oviedo. I would like to pay my greatest gratitude and appreciation to my supervisors, Dr Jorge Garcia Garcia and Dr Cristina Gonzalez Moran of University of Oviedo, for their generous technical support provided while troubleshooting the thesis project.

Special thanks go to Dr Pablo Arboleya, Dr Pablo Garcia for providing me opportunity to pursue postgraduate studies at University of Oviedo. My supervisors dedication, patience, knowledge and experience could not have been surpassed. I admire their guidance towards growing me up academically and personally over last few years.

The personal and administrative support provided by LEMUR group, Dr Islam, Bassam at various stages of my Master thesis degree are acknowledged with gratitude. Timely personal and technical assistance received from Major Umesh & Sujay, cooperate to commission the experimental setup of my master thesis within short period of time. I am very much thankful to them. Thanks also go to my colleagues Umer, Saikot for their valuable input to my research work.

Last but not least, I would like to thank my parents, my sister Swati and rest of family for their unconditional love and continuous support. I would not have been able to complete Thesis without them.

Contents

List of Figures

List of Tables

Glossary

VSI	Voltage source inverter.
PLL	Phase lock loop.
PCC	Point of Common Coupling .
PV	Photovoltaic .
MPPT	Maximum Power Point Controller .
PI	Proportional and integral.
PWM	Pulse width modulation.
LV	Low Voltage .
IGBT	Insulated gate bipolar transistor .
PWM	Pulse Width Modulation.
SVPWM	Space vector PWM.
LCL	Inductor capacitor inductor.
THD	Total harmonic distortion.
PCB	Printed circuit board.
ADC	Analogue to digital converter.
LEMUR	Laboratory for enhanced microgrid unbalance Research.
TCP/IP	Transmission control protocol/Internet protocol.
$\boldsymbol{T_s}$	Sampling time.
$\boldsymbol{T_{sw}}$	Switching time.
$\boldsymbol{P}$	Active power.
$\boldsymbol{Q}$	Reactive power.
$\boldsymbol{V_g}$	Grid voltage.
$\boldsymbol{f_g}$	Grid frequency.
$\boldsymbol{f_{sw}}$	Switching frequency.
$\boldsymbol{P_n}$	Rated power.
$\boldsymbol{V_{dc}}$	DC bus voltage.
$\boldsymbol{L_1}$	Inverter inductor.
$\boldsymbol{L_2}$	Grid inductor.
$\boldsymbol{C_f}$	Filter capacitor.

Chapter 1

Introduction

1.1 Statement of the Problem

This Thesis is basically for LV (Low Voltage) power grid to minimise dependency and the usage of rapidly depleting fossil fuel resources such as coal, and natural gas. It also helps to reduce pollution of fossil fuel based electricity generation and to reduce global warming. Thesis, included simulated technology related regarding single phase grid connected photovoltaic system. Control loop has been used for current and voltage to protect converter if current exceed to some predefined boundary. Integrator has been used to get zero steady state error.

1.2 Research Objectives and Methodologies

Research studies presented in this Thesis focus on grid connected single phase two stage photovoltaic system. Effect of temperature and irradiance on PV and IV curve has been discussed. Variation of irradiance on DC-link voltage, grid voltage, grid current and active and reactive power have been observed. Open loop simulation for PV array, boost converter & full bridge inverter have been started. After having required open loop result, PV array have been synchronised with boost converter including MPPT controller. Dynamic behaviour of grid connected two stage photovoltaic system, inner faster current loop and outer voltage control loop have been designed. A

simulation model of a PV system representing the dynamic behaviour of an actual PV system connected to an LV power grid. Therefore, the dynamic behaviour of all the physical components and all control loops should be accurately modelled. Data sheet for Siliken PV panel given in appendix D.1 and IngeconSun 5TL model have been refered to design simulation model [39].

1.3 Outline of the Thesis

Chapters brief description included in this section. Chapter 2, literature review has been included description regarding solar photovoltaic energy, power converter for integrating PV system to grid, modulation technique, operation and control of VSC and overview of grid connected PV system. Chapter 3 is about system description and modelling of grid connected photovoltaic system. It includes topology and array modelling of photovoltaic system, MPPT algorithm, DC-DC boost converter, voltage source converter, modulation technique, PWM switching, LCL filter & DC link capacitor.

Chapter 4, discussion has been included Simulink model for grid connected photovoltaic system. It includes current and voltage equation photo voltaic array, boost converter with MPPT controller, full bridge inverter with SPWM and simulation of grid connected PV system. Chapter 5 has been covered simulation result regarding photovoltaic array, boost converter with MPPT controller, full bridge inverter with SPWM and grid connected photovoltaic system. Finally in chapter 6, conclusion and future work regarding Thesis has been summarised.

Chapter 2

Literature Review

2.1 Introduction

In most of power generating plants, fossils fuels are main source of energy to generate electricity. Till 19th century energy has been created largely by burning hydrocarbon, oil, coal and natural gas. It produces huge carbon emissions. Emission of greenhouse gases, limited coal resources, environmental distortion, rising prices of fossils fuels and scarcity of foreign exchanges reserves responsible for developing new energy economy. However, energy generation from renewable sources like wind, solar, hydro, biomass, tidal, geothermal, wave, bio-fuels & bagasse does not affect the environment that adversely. Government and electric utility around world has introduced subsidies and significant change in their traditional policies to allow investors to integrate their own renewable power generating systems to electric power grid to promote sustainable energy technologies. Further, commercially attractive rebates, grants and credit schemes will continue to make significant changes to the traditional electrical power grid.

Electrical power generated from a PV system solely depends on factors such as solar irradiance and ambient temperature. These factors are subjected to sudden or slow variations, resulting in changes in the output power. As PV systems are interfaced to LV power grids through power electronic converters (inverters) and as no mechanical inertia is involved, changes in power flow can take place in relatively short

periods. Such changes can cause rapid voltage fluctuations at the point of common coupling (PCC) of a PV system and can lead to overvoltage, under-voltage and/or flicker problems. Further, switching frequency and low-order harmonic levels may increase with the addition of PV systems to LV power grids, possibly deteriorating the quality of power supply.

Simulation studies can be performed to investigate the terminal characteristics of a PV system under different operating conditions and to analyse how LV power grids will behave when multiple PV units are integrated. In order, to perform such simulation studies, the development of accurate simulation models of PV systems is necessary. A detailed simulation model of a PV system that represents the dynamic behaviour of all the physical components of a grid-connected PV system and the associated control loops are essential to investigate the dynamic behaviour of a single or multiple grid-connected PV system under different operating conditions.

2.2 Solar Photovoltaic Energy

All photovoltaic (PV) cells consist of two or more thin layers of semi-conducting material. It is mostly silicon. Electrical charges are generated, when semiconductor exposed to sunlight. It produces direct current when multiple cells are connected.

2.2.1 Types of Photovoltaic cell and Equivalent circuit of a PV cell

PV panels are of different types like monocrystalline, polycrystalline, thick-film silicon [39]. Monocrystalline cells sliced from a single crystalline crystal of silicon. It is typically converting around 15 % of sun's energy into electricity. Manufacturing process is slightly complicated so cost is high. Polycrystalline cells cut from an ingot of melted and recrystallized silicon. The ingots are then saw cut into very thin wafers. Then it assembled into complete cells. They are cheaper than monocrystalline. But less efficient as they converting 12 % of suns energy into electricity. In thin-film

silicon panels silicon is deposited in continuous process onto base material giving fine grained, sparkling appearance. Then it is encapsulated in transparent insulating polymer with tempered glass cover and then bound into metal framed module. In this case, monocrystalline panel SLK72M6L of SILIKEN has been used D.1 [38] [39]. A panel is 72 series cells. The peak power is between 285 Wp to 310 Wp.

The equivalent circuit of PV cell is shown in figure 2-1 b. Internal losses of current in model has been ignored. A diode is connected in anti-parallel with current source. When PV cell exposed to sunlight DC current is generated is denoted by I. By using Kirchhoff law output current, I can be obtained by equation 2.1,

$$I = I_{ph} - I_D = I_{ph} - I_{sat}[e^{\frac{V+IR_s}{V_t}} - 1] \tag{2.1}$$

In case of short circuit situation, the equation presented in 2.1 can be rewritten as:

$$I_{sc} = I_{ph} - I_D \tag{2.2}$$

where

I_{sc} : Short circuit current (A)

I_{ph} : Photo current (A)

I_D : Diode current (A)

I_{sat} : Saturation current (A)

V_t : Thermal voltage (v)

R_s : Series resistance (Ohm)

V : Terminal voltage (V)

I : Output current (A)

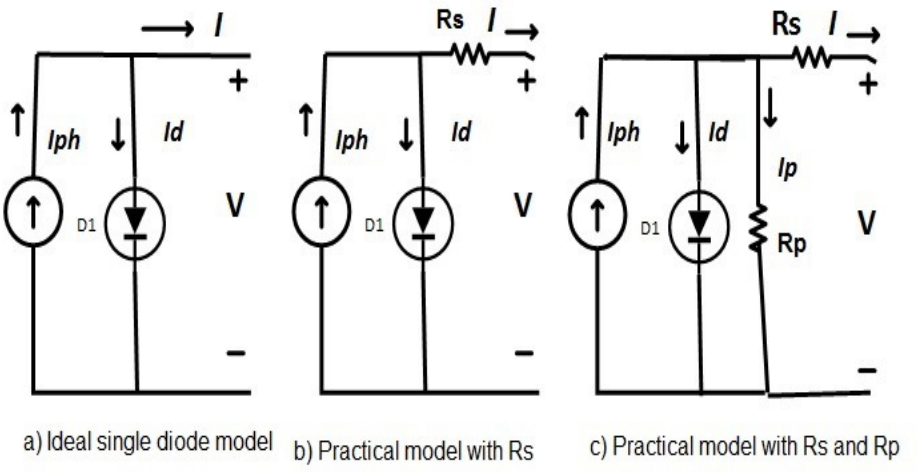

Figure 2-1: shows Equivalent circuit of a solar cell and PV device [3].

2.3 Power Converters for Integrating PV Systems to the Grid

Power converter system is used to convert DC power from PV array to AC power. DC-DC power conversion stages have been avoided with careful selection of the PV array to closely match with the required DC voltage needed for inverter. This may not be always possible with small capacity PV installations which may need to boost the output voltage of the PV array. For integrating to grid in such situation, DC-DC boost converter has been used to boost the output voltage of the PV array as suitable for integrating to the grid. However, grid connected inverters are carefully designed to mitigate the problems with DC current injection, islanding, flicker and harmonics.

Further converters can be classified as per the commutation process used in the design. It can be as either line commutated converters or force commutated converters. Based on voltage and current waveforms at their DC-links, DC-AC converter can further be classified as voltage source converters or current source converters (CSC). In a VSC, DC-link terminals are connected in parallel with a relatively large capacitor. And polarity of the DC-link current of the converter determined direction of average power flow. In a CSC, DC-link terminals are connected in series with a relatively large reactor. And the polarity DC-link voltage of the converter determined

direction of average power flow.

To control the power flow through a CSC, it should be designed from fully controllable bipolar power electronic switches. The power flow of a VSC can be fully controlled if the converter is made of reverse conducting power electronic switches IGBT or MOSFET. These switches basically used for low power converter application. That is reason VSC converter become most widely used type power electronics converter to interfaces low power PV system to grid.

In this dissertation, single phase two stage DC-DC-AC converter has been used. DC-AC inverter in single phase full bridge transformer less inverter is usually preferred for relatively small domestic rooftop PV installations.

2.4 The Modulation Techniques

Single phase voltage source converter has been used for H bridge bipolar or unipolar modulation method. By controlling the magnitude and the angle of voltage at the output of the H-bridge, v, of the VSC with respect to the grid side voltage, v_g, amount of power injected or absorbed has been controlled. Basic structure of Single-phase VSC has been shown in figure 2-2.

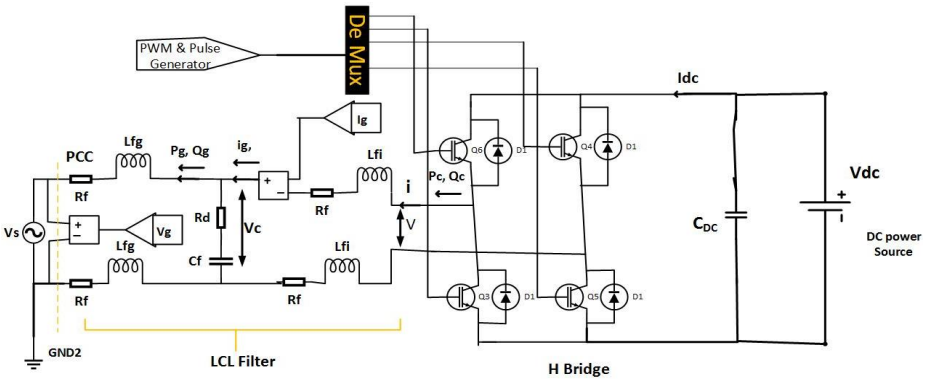

Figure 2-2: Basic structure of Single-phase VSC[30].

To generate a desired voltage at the output of the H-bridge, Sinusoidal pulse-width modulation (SPWM) techniques has been used. There are two SPWM technique bipolar-SPWM and unipolar-SPWM used in VSCs. The magnitude of modulation

signal(m) is proportional to magnitude, phase angle and frequency of voltage that should be generated at the output of the H-bridge. Sinusoidal signal is compare with high frequency triangular signal using relational operator to get pulse-width modulated switch-ON and switch-OFF pattern. It is shown in figure 2-3 a and b. The switching pattern is then applied to the power electronic switches of the H-bridge shown in figure 2-4 and figure 2-5. The current injected by the VSC to the grid is highly distorted. Filtering mechanism has been used in order minimise the distortion in current.

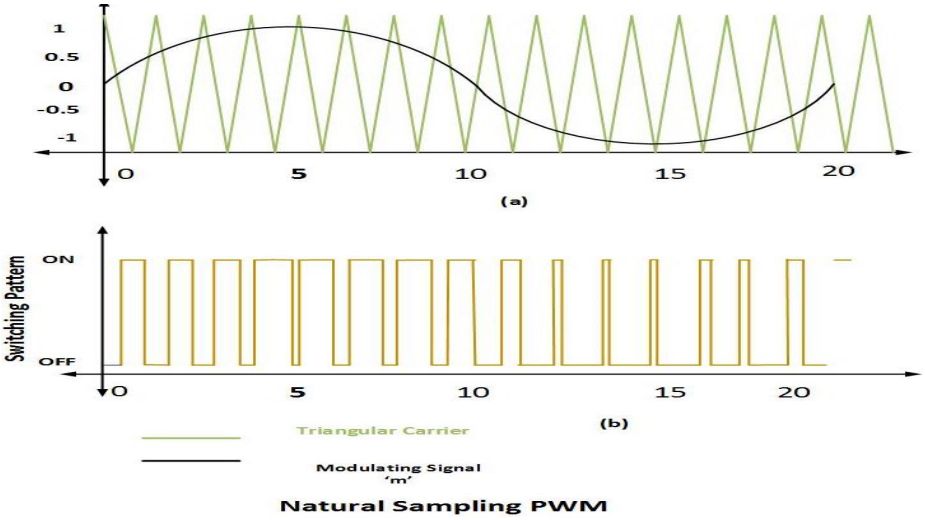

Figure 2-3: Shows Generation of PWM switching pulses[30].

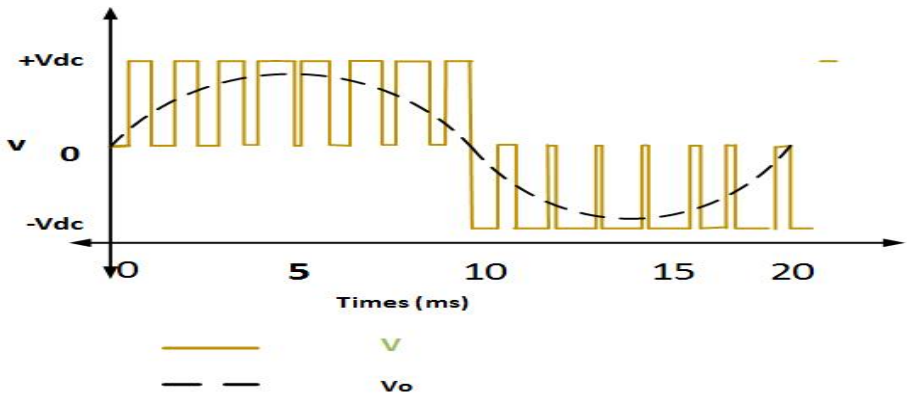

Figure 2-4: shows Output voltage of a H-Bridge of a VSC that uses unipolar-SPWM technique [30].

The advantage of unipolar modulation is that it has high efficiency up to 98 %

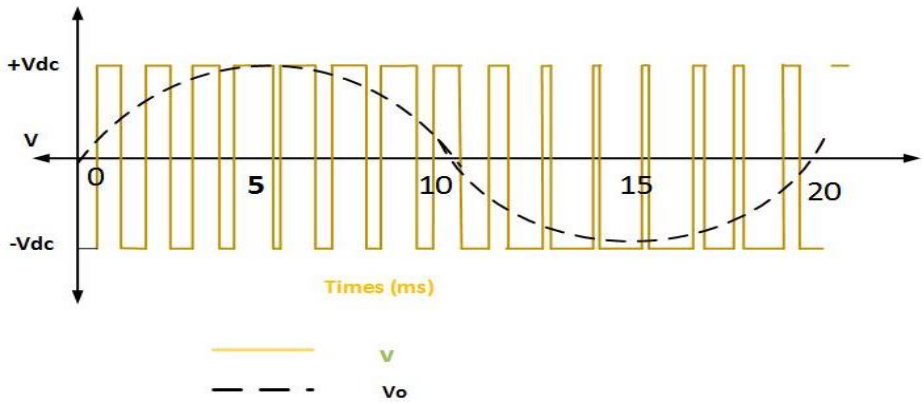

Figure 2-5: shows Output voltage of a H-Bridge of a VSC that uses bipolar-SPWM technique [30].

due to reduced losses during zero voltage states and low losses in the output filter. The advantage of bipolar modulation is that there is no switching harmonics, very low leakage current and EMI

Disadvantage of bipolar modulation is lower efficiency up to 96.5 % due to reactive power exchange between L_{dc} and C_{pv} during freewheeling. Disadvantage of unipolar modulation is switching harmonics, high leakage current and EMI [29].

Other technique which is largely used in power electronics is space vector Pulse width modulation (SVPWM). Space vector PWM control scheme for three-phase PWM inverter in PV generation system discussed in Jiyong Li et al. [34]. From Vdc input voltage of the inverter, we can calculate each state voltage. Once voltage in reference frame is determined, duration period T1 and T2 time for each vector in each PWM cycle has been calculated. Low total harmonic distortion (THD), constant switching frequency, well-defined output harmonic spectrum, optimum switching pattern and excellent dc-link voltage utilization are advantages with SVPWM. In Q. Zeng et al. [6] explained drawbacks for SVPWM [31].

2.5 Operation and control of VSC

2.5.1 Basic Operation of a VSC

To reduce ripple in output current, VSC is integrated to grid via. coupling inductor. It also minimises the effect of the PWM switching voltage developed at the output of a VSC. To improve limited capability of attenuating switching current ripple of VSC, LCL filters often used in grid-connected VSCs. LCL filter which shown in figure 2-6, attenuates high frequency switching ripple current of VSC. LCL filter design also affect dynamic performance of control system of grid connected VSC. While designing LCL filter accuracy should be high. In detail procedure of LCL filter also explain in appendix B.

2.5.2 Control Systems in a VSC

Based on control method, VSC can be classified as either voltage or current controlled. By adjusting the phase angle and the magnitude of the output voltage of the VSC relative to the PCC voltage, real and reactive power output are controlled. Due to lack of close loop to control its output current, there is no over current protection in VSC. But in case of current-controlled VSC the output current of the VSC is controlled. The control of the active and reactive power outputs is achieved by controlling the output current. By adjusting the magnitude and phase angle of the output voltage of the VSC with respect to the grid voltage, current has been controlled. In a current controlled VSC, the closed-loop current controller and grid synchronisation mechanism are the two main control systems being used to integrate PV systems to the grid.

2.6 Grid-Connected PV System

Grid synchronization is mechanism, where VSC has been synchronize to grid. This mechanism also used for generating an accurate current reference signal to inject the desired amount of active and reactive power to grid. Method choose for synchronization depending on application and type of current controller used. One of the

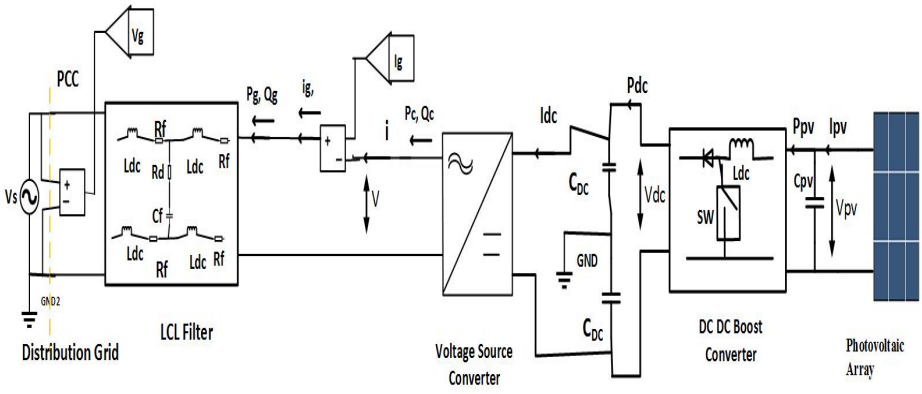

Figure 2-6: shows Grid connected VSC with LCL filter and PV System [30].

simplest grid synchronization method is voltage zero crossing detection. Dynamic performance of voltage zero crossing detection is quite low because it fails in the presence of harmonics in the grid because of multiple zero crossings [40] [7]. For a single-phase VSC, synchronous reference frame based PLL (s-PLL) has been used [7] [4]. In this method, the peak value of the measured grid voltage can be obtained easily.

Chapter 3

System Description and Modelling of Grid Connected Photovoltaic System

3.1 Array Modelling of Photovoltaic Systems

In this chapter simulation studies of the power converter is conducted in Simulink platform. Different operational scenarios are discussed with their simulation results to support the design objective of the system. The first part of this chapter defines the key parts of the simulation model and the second part deals with simulation results.

3.1.1 Model of Photovoltaic Module

Equivalent circuit of solar cell with one diode and some equation has been discussed in chapter 2. Equation which responsible for output current I and diode current I_d, discussed in chapter 2. In this chapter, equation and mathematical equivalent circuit has been derived for photovoltaic array.

The topologies are characterized to calculate several unknowns. It classified with respect to total number of unknowns. Normally the single diode model is known as five parameter model. And other one double diode is known as seven-parameter

model. Both model based three characteristic points of the current-voltage (I-V) curve i.e. open-circuit condition, short-circuit condition, and MPP [26] [37]. Five characteristics has been considered midway between MPP and open-circuit condition, at one-half of the open circuit condition [18]. For these models, mathematical-based equation has been used and cannot be used directly in a circuit simulator. Considering the environmental conditions (ECs), mathematical models of a PV cell has been derived. While designing model, parameters has been used usually available in Siliken SLK72M6L manufacturers PV module datasheet [38].

Correct value of the parameters R_s , R_p, I_{sat}, I_{ph} under the actual ECs are not available at all in the datasheets of the PV modules. This parameter can be used in equation 3.2, after determining correct value of above parameter. Under standard test condition short-circuit current (I_{sc}), open-circuit voltage (V_{oc}), voltage and current in MPP (V_{mpp} & I_{mpp}), maximum power (P_{MPP}), coefficients (ΔI_{sc}) (temperature coefficient for the short circuit current) and (ΔV_{oc}) (temperature coefficient for the open circuit voltage) these parameters are defined. Diode current can be neglected and can be very small in comparison with I_{sc}. Photo current I_{ph} is equal to I_{sc} current can be expressed as each irradiation as cell temperature as,

$$I = I_{ph} - I_D = I_{ph} - I_{sat}[e^{\frac{V+IR_s}{V_t}} - 1] \tag{3.1}$$

$$I_{ph}(G_a, T) = I_{scs} * (Ga/Gas) * [1 + \Delta I_{sc} * (T - T_s)] \tag{3.2}$$

I_{scs} : Short Circuit Current in Standard Test Conditions (STC)

G_a : Irradiance (W/m^2)

T : Cell Temperature (K)

G_{as} : Standard Irradiance (1000 W/m^2)

T_s : Standard Cell Temperature (298 K)

ΔI_{sc} : Short circuit current coefficient with temperature (1/K)

T is cell temperature obtained from weather condition. $NOCT$ normal operation cell temperature get by using the following expression:

$$T = (T_{op}) + (NOCT - (T_n)) * (\frac{G_a}{G_{an}}) \tag{3.3}$$

where T_{op} : Operating Ambient Temperature (K)

T_n : Operating Normal Temperature (293 K)

T_n : Normal Irradiance (800 W/m^2)

In the open circuit situation, open circuit voltage can be calculated using equation 3.4.

$$V_{oc}(T) = V_{ocs} + \Delta V_{oc}(T - T_s) \tag{3.4}$$

where,

V_{oc} : Open Circuit Voltage (V)

V_{ocs} : Open Circuit Voltage in STC (V)

ΔV_{oc} : Open Circuit Voltage Coefficient with Temperature (V/K)

$$I_D(G_a, T) = I_{ph}(G_a, T) = I_{sat}(G_a, T) * [e^{\frac{V_{oc}(T)}{V_t(T)}} - 1] \tag{3.5}$$

$$V_t(T) = A * K * \frac{T}{q} \tag{3.6}$$

Where equation 3.6 is the thermal temperature (V), A the diode ideality factor, q the charge of an electron and k the Bolztman constant. With equations 3.1 to 3.6 the operating point for each pair of irradiance G_a and room temperature T_{op} can be determined, once A and Rs are known.

Manufacturer of the solar module gives another parameter needed to model the solar cells. The datasheet which gives the electrical characteristics is calculated under standard test condition STC when the temperature T is 25° and the irradiance G is 1000 W/m^2.

Matlab Simulink I-V model has been constructed using all equation. Technical characteristics sheet provided by manufacturer for monocrystalline SLK72M6L SILIKEN panel given in table 3.1. Panel has series of 72 cells. The peak power per

Table 3.1: Technical Characteristics for SILIKEN SLK72M6L

Parameter	Value
Short circuit current I_{sc} (A)	9.02
Open circuit voltage V_{oc}	44.5
Current at maximum power point I_{mp}	8.51
Voltage at maximum power point V_{mp}	35.8
Number of cells in series n_s	6
Temperature coefficient of I_{sc}	$1.9780*10^{-05}$
Temperature coefficient of V_{oc}	$-5.8608*10^{-05}$
P_{max}(Wp)	305

panel 305 (Wp) per panel, short circuit current coefficient, open circuit voltage coefficient with temperature and other parameter of panel measured in Standard Test Condition (STC) given in table 3.1. For this experiment, 12 panel i.e. six set of two array connected in parallel. In this case, array voltage and current have been calculated from equation 3.1. This array voltage has been used as input to boost converter.

3.1.2 Curves IV Characteristics of PV Array

The current to voltage characteristic of a solar array is non-linear, which makes it difficult to determine the MPP. The Figure 3-1 & 3-2 gives the characteristic I-V and P-V curve respectively for fixed level of solar irradiation and temperature.

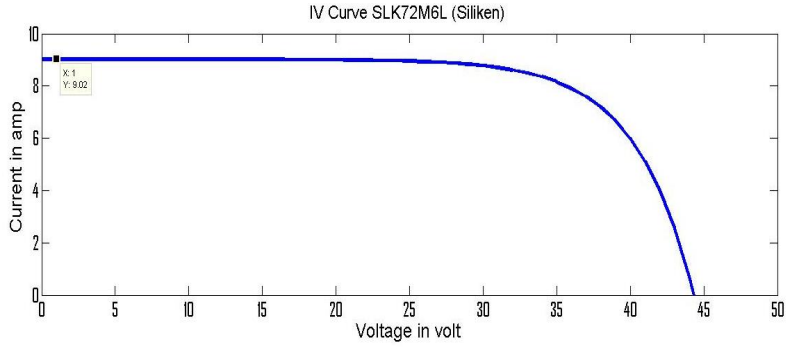

Figure 3-1: I-V characteristic of a solar array for a fixed temperature & irradiance [31] [38]

The characteristic I-V curve 3-1 shows that there are two regions in the curve: one is the current source region and another is the voltage source region. In the voltage

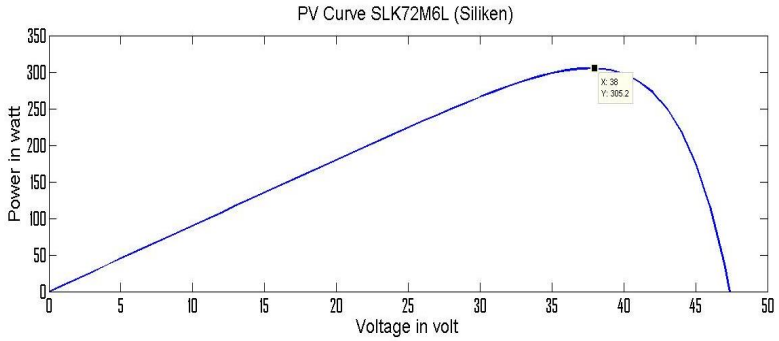

Figure 3-2: P-V characteristic of a solar array for a fixed temperature & irradiance [31]

source region (in the right side of the curve), the internal impedance is low and in the current source region (in the left side of the curve), the impedance is high. Irradiance & temperature plays an important role in predicting the I-V characteristic and effects of both factors should be considered while designing the PV system. Whereas the irradiance affects the output current, temperature mainly affects the terminal voltage [5] [30].

3.2 MPPT Algorithm

Nonlinear solar cell I-V characteristic changes with irradiation and temperature. It is difficult to track unique point for the maximum power (P_{MPP}). With help of optimal voltage V_{mpp} and the optimal current I_{mpp}, maximum power (P_{MPP}) has been located. MPPT draws maximum power from the solar array regardless of weather or variations in load conditions. There are diverse MPPT algorithms that have been manufacturing for PV systems [9] [27].

Because of the simplicity in the algorithm, perturb and observe (P&O) method has been identified as a simple MPPT algorithm. It needs only one sensor. The P&O method has been identified as a slow tracking algorithm compared to other available MPPT. In the occurrence of rapid variations of the environmental conditions, it fails sometimes [8]. P&O method is not working properly in case of continuous oscillations around the MPP. Other MPPT algorithm is the incremental conductance

(InC) method. As compared to P&O method, the InC method tracks the MPP quickly and accurately [11]. InC method is working properly in case of continuous oscillations around the MPP as compared to P&O method. It requires output current and voltage feedback of the PV array needed to implement. The InC method is accurate, less complex and easily implementable MPPT algorithm.

In P&O or InC method, firstly output voltage and current of PV module has been measured. Then control parameter needs to be increased or decreased, once PV power has been observed. Reference signal (voltage and current) or duty ratio as controller for switching signal has been used for DC/DC converter. P&O MPPT algorithm used in this thesis, does not require previous knowledge of the PV module characteristics. DC-link capacitor has been calculated correctly to work MPPT algorithm correctly. Switching frequency and step size has also been selected properly as it affecting algorithm. In section 3.2.1, searching algorithm, their flow chart and theory has been discussed.

3.2.1 Perturbation & Observation

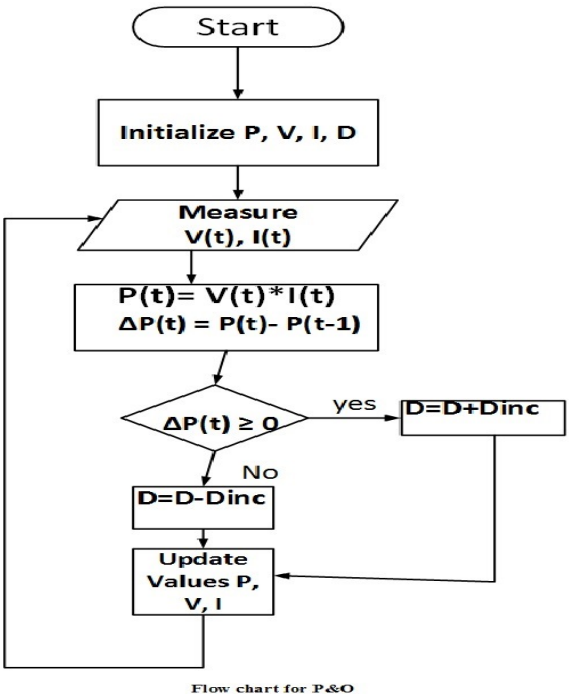

Figure 3-3: Flow chart for P& O [8]

Perturb & Observe algorithm flow chart has given in the figure 3-3. It states that when the operating voltage of the PV panel is perturbed by a small increment and if the resulting change in power P is positive, then direction of MPP followed. Or else keep on perturbing in the same direction. If P is negative, then direction of MPP not followed. The sign of perturbation supplied must be changed in this case.

In this algorithm, voltage for PV array has been used as sensor. So, the cost of implementation is less and hence easy to implement. The time complexity of this algorithm is very less. By reaching very close to the MPP it does not stop at the MPP and keeps on perturbing in both the directions. When the algorithm has reached very close to the MPP and appropriate error limit has been set or can used a wait function. It ends up increasing the time complexity of the algorithm.

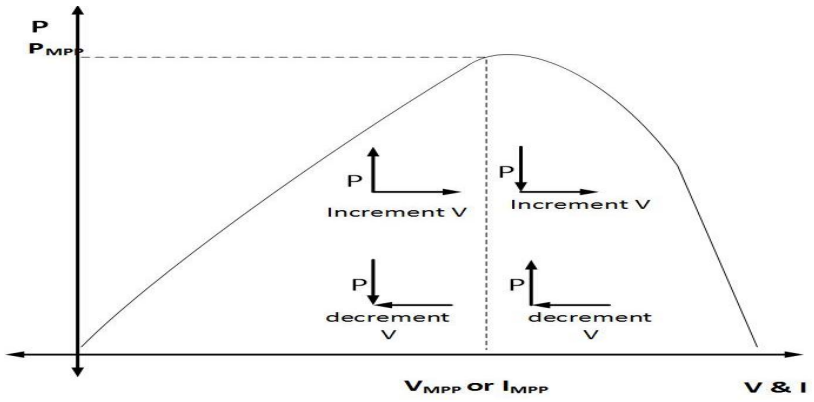

Figure 3-4: Principle of P& O [8]

In figure 3-4, on the left of the MPP, while incrementing the PV voltage, power of the PV increases. By decrementing the PV voltage, the power of the PV decreases. On the right of MPP, incrementing the voltage decreases the power and decrementing the voltage increases the power. To extract the maximum power from the PV module, MPPT controller has been implemented. Detail explaination regarding Incremental & Conductance method explained in reference [22] [8].

3.3 DC-DC Boost Converter Operation

Output voltage of boost converter is always greater than input voltage so it is also called step up converter. Boost converter has high efficiency only for reasonable gains and for low power values.

3.3.1 Mode 1:Operation of the Boost Converter

Inductor gets charged through the DC source i.e. PV panel and stores the energy, when switch is closed as shown in figure 3-5. Inductor charges linearly because output DC source is constant due to large C. The diode blocks the flowing current and so the load current remains constant. Current is being supplied to load due to the discharging of the capacitor. Selection of input capacitor, inductor, output capacitor and load resistor explain in appendix A.1.

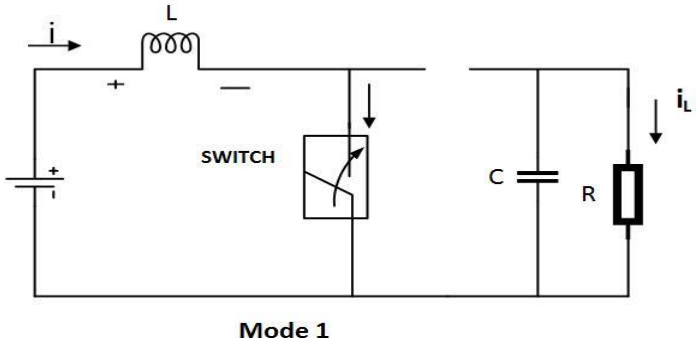

Figure 3-5: Circuit diagram of boost converter (mode 1) [32].

3.3.2 Mode 2:Operation of the Boost Converter

In mode 2, figure 3-6 the switch is open. So, the diode becomes short circuited. The energy stored in the inductor gets discharged through opposite polarities. Discharging of inductor charge the capacitor. Throughout the operation, the load current remains constant. Boost converter works properly because output C is very large. Due to large C, variations in current ripples do not affect output voltage. Figure 3-7 shows the waveforms for a boost converter.

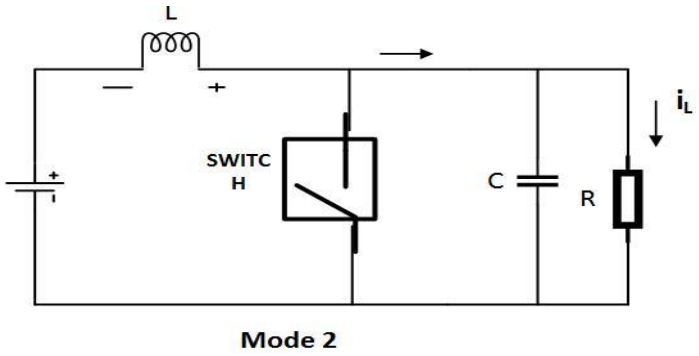

Figure 3-6: Circuit diagram of boost converter (mode 2)[32].

3.4 Modulation Technique of Single Phase Full Bridge VSC

Figure 3-8 & 3-10 shows a simplified circuit diagram and output Voltage Waveform of a Single-Phase H Bridge inverter. The logic behind the switching of the devices is given below,

When S1 and S2 are turned on $+V_{dc}$ is obtained at the output
When S3 and S4 are turned on -V_{dc} is obtained at the output
When S1 and S3 or S2 and S4 are turned on together zero voltage is obtained at the output
Output voltage level changes between either 0 to -V_{dc} or from 0 to $+V_{dc}$ in unipolar switching scheme. Advantage of unipolar scheme is that, it has the effect of doubling the switching frequency as far as the output harmonics are concerned. Using bipolar or unipolar modulation schemes, an AC output voltages V_{ab} has been adjusted. In thesis, unipolar modulation has been included for H Bridge inverter. In unipolar scheme, the triangular carrier waveform is compared with two reference signals which are positive and negative signal. The basic idea to produce SPWM with Unipolar voltage switching is shown in figure 3-9. Output voltage switching characteristics for unipolar switching shown in figure 3-11. Figure 3-12 shows the sine wave and triangular wave control signals respectively. Detail explanation regarding unipolar voltage switching signal is given in reference [12] [28] [17].

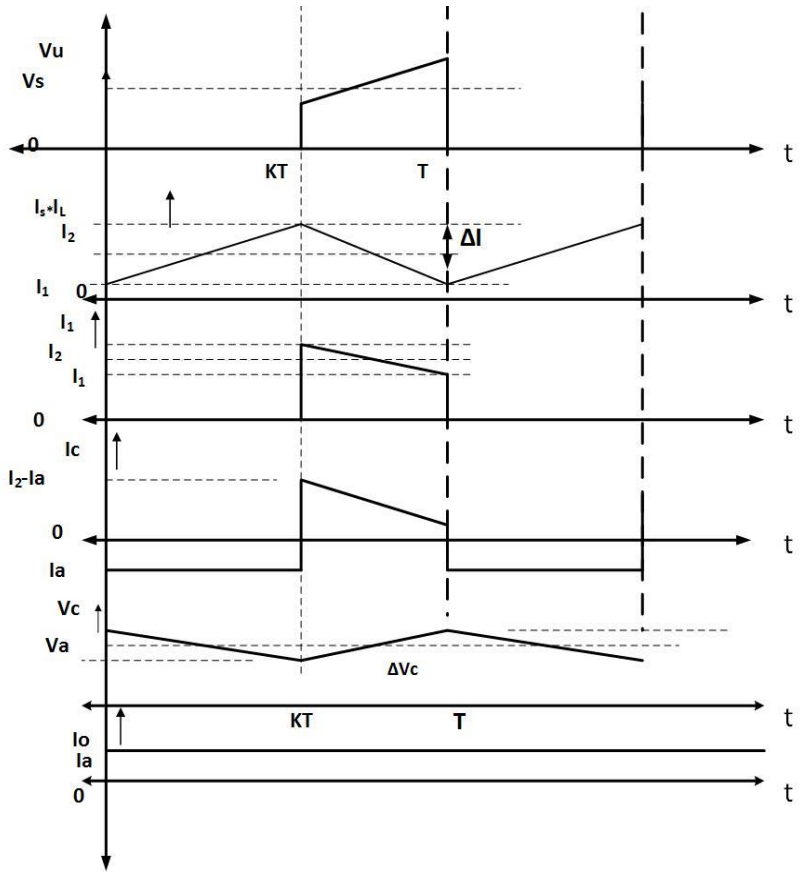

Figure 3-7: Wave form of boost converters operation[32].

3.5 LCL Filter

The values of the inductors and the capacitor of the LCL filter of the PV system shown in figure 3-13 were determined as $L_i = 3 * 10^{-3}$ H, $L_g = 1.5 * 10^{-3}$ H and $C_f = 2.6 * 10^{-6}$ F, by following the design guidelines established in [1]. Resistances of inductances L_{fc} and L_{fg} are assumed as $R_{fc} = 0.5$ Ohm. The total inductance of the designed LCL filter is less than 0.1 pu (using a base - $S_b = 5e4$ kVA, $V_b = 230$ V) and the resonant frequency, f_{res}, is 10.7 kHz; less than $0.5 f_{sw}$. A damping resistor $R_d = 1.5$ Ohm, calculated as one third of the impedance of C_f at f_{res}, is added in series with C_f to improve the stability of the current controller [21]. Detail design for LCL filter explain in appendix B.

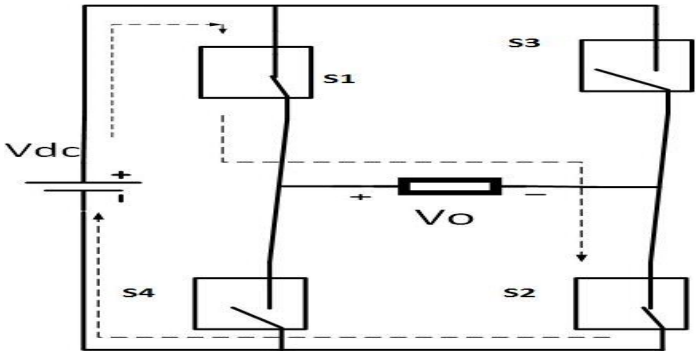

Figure 3-8: Output current for S1, S2 ON; S3, S4 OFF for $t1 < t < t2$ [32].

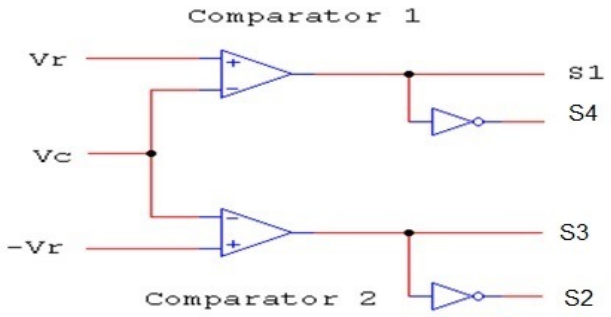

Figure 3-9: Unipolar PWM generator [12].

3.6 DC-link Capacitor

The output capacitance of a power converter is a vigorous part of the overall system. It maintains the output voltage. It affects stability of the regulator. The component parameters are part of the feedback control loop. Using DC link capacitor value, reference d and q axis current has been designed. These references has been used for further PWM signal. The output capacitance determines the position the dominant pole. It therefore affects the stability boost converter. Output voltage ripple of the converter has been affected by output capacitor. The output voltage peak-to-peak ripple ΔV_{dc} given by equation 3.7.

$$\Delta V_{dc} = \frac{P}{(C_{dc} * V_{dc} * \omega)} \tag{3.7}$$

Practically, it is impossible to reduce DC-link voltage ripple to zero. Ideally in simulation zero ripple has been observed for large capacitor value. There is always

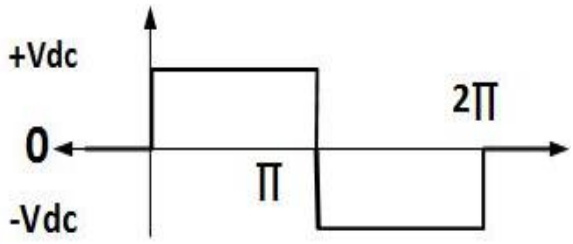

Figure 3-10: Output Voltage Waveform [32].

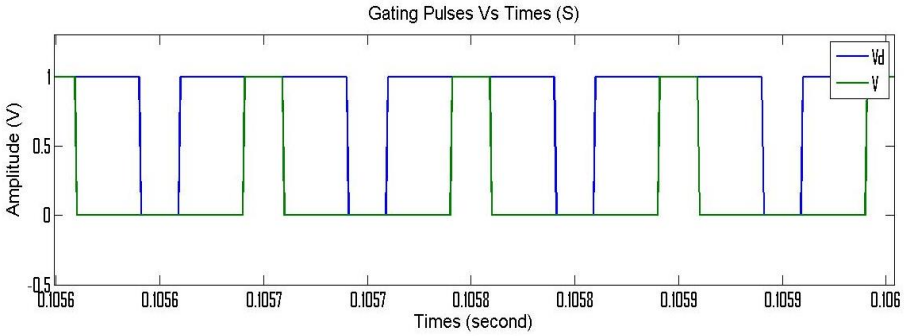

Figure 3-11: shows Waveform for SPWM with Unipolar voltage switching [25].

voltage ripple in DC link voltage of single phase VSC. It calculated to limit peak-peak ripple of DC-link voltage. ΔVdc is average 5 or 2 % of Vdc_{avg}. An excessively large capacitor at the DC-link can reduce the DC-link voltage ripple almost to zero as per 3.7. But that is practically impossible and there is a limitation to the size of C_{dc}. Hence there is a voltage ripple in the DC-link voltage of a single-phase VSC. The capacitance of the DC-link capacitor of a single-phase VSC has been determined to limit the peak-peak ripple of the DC-link voltage. The detailed design procedure of the DC link capacitor described in appendix A.1.2. V_{dcavg} = 400 V, ΔV_{dc} =0.05 * 400 =20 V. Selected C_{dc} =2.5 mF.

3.7 Control system in VSC

Grid synchronization is important feature of grid side converter control. Synchronization algorithm can detect the phase angle of grid voltage to synchronize the delivered

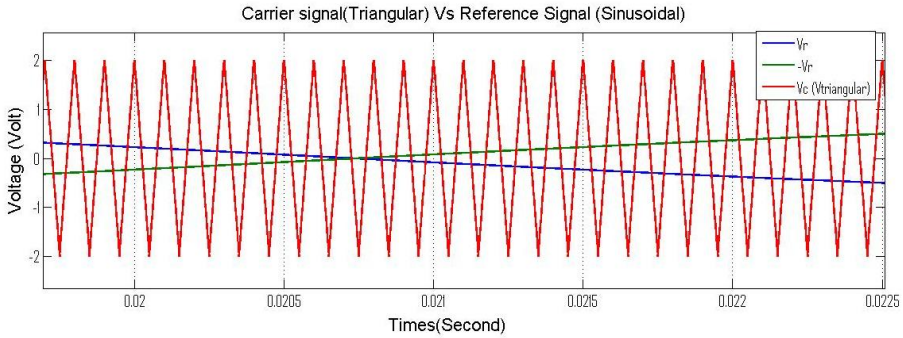

Figure 3-12: shows Carrier and Reference Waveform for SPWM with Unipolar voltage switching [25].

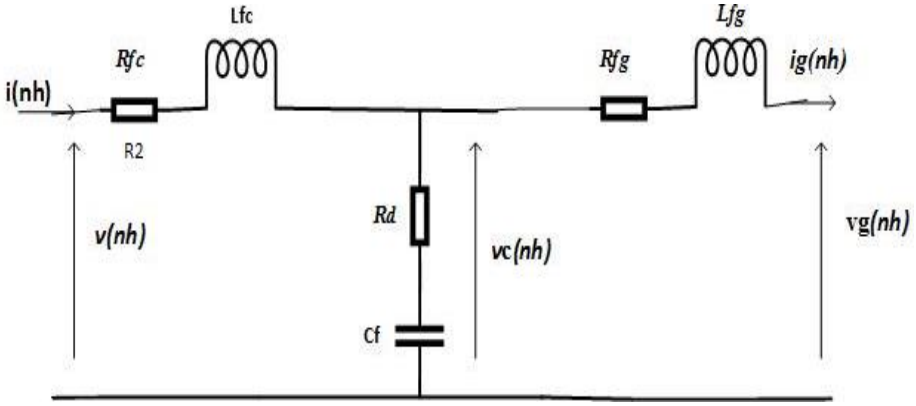

Figure 3-13: shows LCL filter [30].

power. This method is used to synchronize the inverter output current with the grid voltage, to obtain a unity power factor. It has been developed to create a current reference that consists of active and reactive components.

The design of the control system for the inverter has been divided into current controller, DC voltage controller and grid synchronization. A schematic block diagram of the controller is shown in figure 3-14. Current controller control AC current injected into the grid and voltage controller control DC voltage. The single-phase feedback current loop is used to regulate the grid current. The current controller loop and the model as shown in figure 3-15.

Stationary reference frame component alpha has been created by delaying grid voltage/current component using integer delay block in Simulink. And orthogonal component beta has been created by further delaying alpha component. Grid angle is calculated as shown in figure 3-18. Grid angle has been used in park transformation

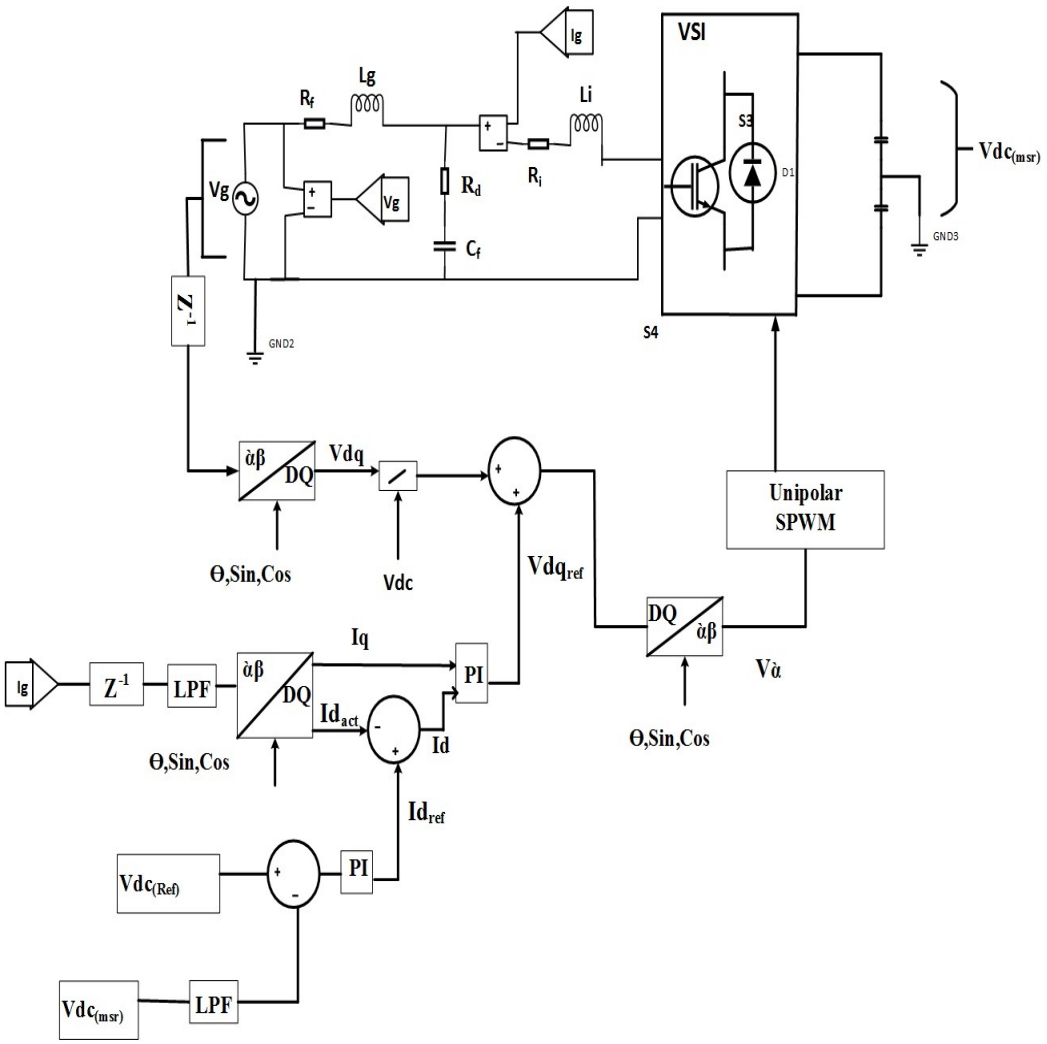

Figure 3-14: shows Schematic VSI including voltage and current control loop [43].

for calculation of DQ rotating reference frame component [43]. Figure 3-17 shows the two orthogonal stationary component waveforms formed in the single-phase system. It has been observed that V_β is effective after 0.025 sec which represents a quarter-cycle delay from V_α.

DC-link film capacitor producing significant double line frequency ripple. Low pass filter with 100 Hz cut off frequency has been used to filter V_{dcmsr}. LPF minimises ripple. Error between measured and reference DC linked voltage has been pass through PI to get I_d reference current. Error between I_{dref} and I_{dact} has been again passed through PI to get V_{dref} d-axis voltage. V_{dqref} dq-axis voltage has been further used as feed forwarder. After final addition, $V_{dq(total)}$ passed through Inverse Park

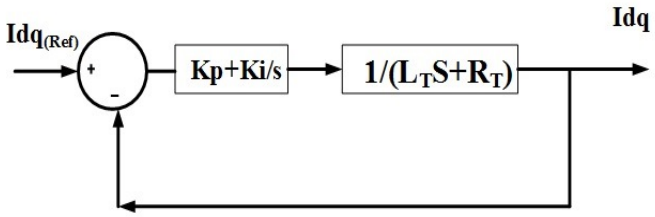

Figure 3-15: shows Current control loop [43].

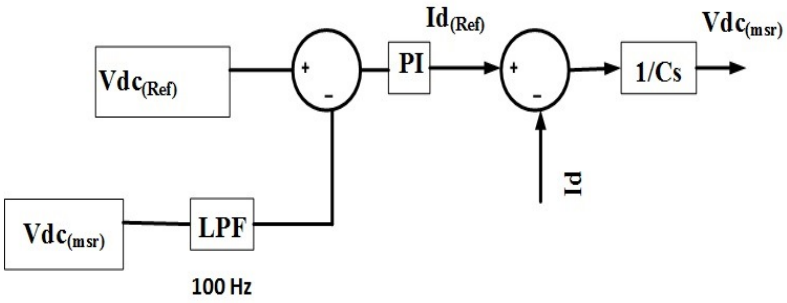

Figure 3-16: shows DC Voltage control loop [43].

transformation block i.e. DQ-$\alpha\beta$ block. $V\alpha$ is real part of this voltage has been used for Unipolar SPWM. The feed-forward signal employed while generating SPWM to minimize drawback of slow dynamic response of cascade control.

In thesis PI with pole zero cancellation has been designed in a DQ synchronous frame. It can achieve zero steady state error at the fundamental frequency. It also improves its dynamic response. But this method is not readily applicable to single-phase power converters because there is only one phase variable. AB to DQ transformation needs at least two orthogonal variables which do not have in case of single phase power converter. Imaginary orthogonal circuit concept has been introduced to get other variable. The imaginary Orthogonal Circuit has the same circuit components and parameters e.g. power switches, inductors and capacitors. Imaginary circuit variable like inductor current and capacitor voltage maintain 90° phase shift with respect to their counterparts in Real circuit.

So, for simulation, $\frac{1}{4}$ cycle delay method has been used. Stationary reference frame have been constructed using delay method explain in figure 3-19. And then this alpha and beta has been used as real and imaginary signal respectively to convert it into

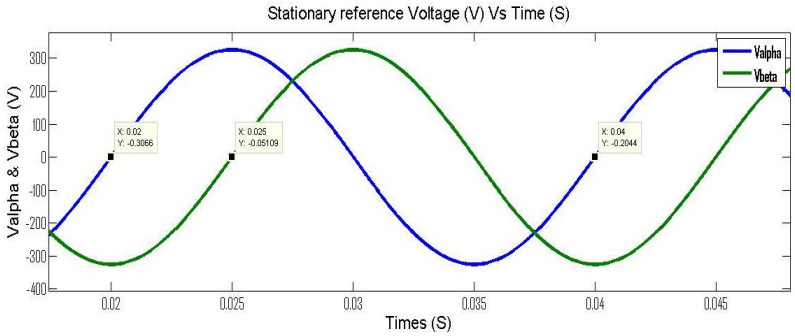

Figure 3-17: shows MATLAB/SIMULINK results for real and imaginary phase waveforms [36].

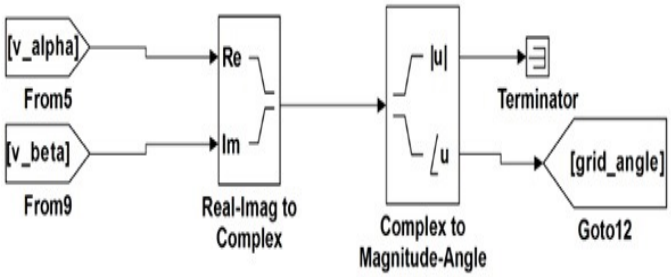

Figure 3-18: shows Grid angle Calculation [36].

complex variable. This complex signal has been used to get grid angle and magnitude. This grid angle has been used further for alpha-beta stationary reference signal to rotating DQ reference signal. Grid angle has also been used in Park transformation and Inverse Park tranaformation. At the fundamental frequency, controller can be designed and easily implemented in the rotating DQ frame to achieve a theoretically infinite control loop gain.

In coming section, discusion has been regarding construction of Imaginary Orthogonal circuit, controller design for the single-phase power converters in the DQ rotating frame and final conversion of control signal from the rotating frame to the stationary frame for the Real Circuit. Real circuit and its imaginary circuits shown in figure 3-20.

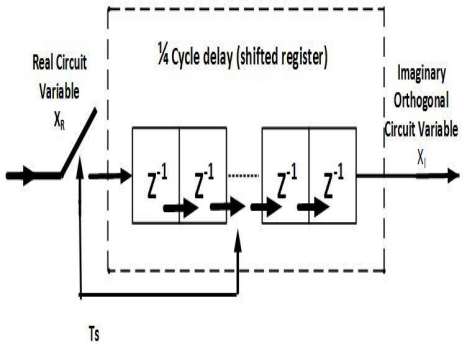

Figure 3-19: shows Construction of the imaginary Orthogonal Circuit Variables [41].

Construction of Imaginary Orthogonal Circuit Variables

Imaginary Orthogonal Circuit does not physically exist; orthogonal Circuit variables can be constructed by using the Real Circuit variables. Imaginary Orthogonal circuit variable and the real Circuit variables has fixed 90° phase shift. Imaginary signal, delay by quarter cycle using integer delay block in Matlab Simulink as shown in figure 3-19. Real & Imaginary circuit variable is denoted by alpha & beta component respectively.

Figure 3-21 shows that Imaginary Orthogonal Circuit is estimated from the Real Circuit and it introduces the dynamics of a quarter cycle delay in this construction process. In result shows that delay does not affect the control accuracy in steady state. It has guaranteed zero steady state error. As compared to conventional approach, dynamic response of the control is still much faster. In case of unknown or variable fundamental frequency application, phase lock loop can be used to track the line frequency. In case of Imaginary Orthogonal Circuit, PLL dynamics need to be included.

DQ rotating frame for controller design is like that of DC-DC converters. Imaginary Circuit variables are build using the Real Circuit variables. Complex real and imaginary block has been used in Matlab Simulink. Then complex to magnitude-angle block, grid angle has been calculated which used in DQ transformation block. Then, the variables in the RI stationary frame are transformed into the DQ rotating frame. Then voltage and/or current signal designed in the rotating DQ frame has

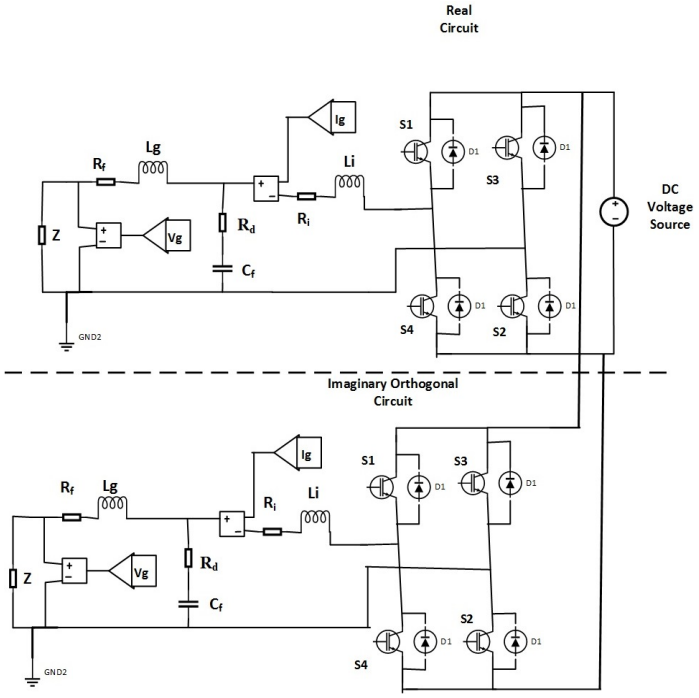

Figure 3-20: shows Real Circuit and its Imaginary Orthogonal Circuit [41].

been converted to real and imaginary stationary frame. For this conversion, inverse transformation matrix has been used. Imaginary frame signal has been discarded. Real signal as reference signal has been used for Unipolar modulation scheme. Triangular signal has been used as carrier signal. Frequency of triangular signal is around 10 Khz.

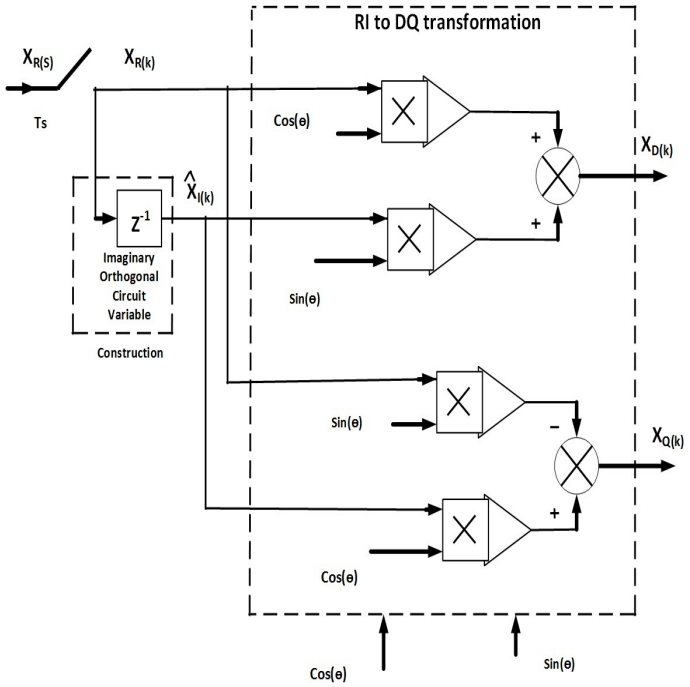

Figure 3-21: shows DQ transformation using constructed Imaginary Orthogonal Circuit Variable for fixed fundamental frequency application [41].

Chapter 4

Simulation of Grid Connected Photovoltaic System Using Matlab / Simulink

4.1 Simulation of Photovoltaic Array

MATLAB based model shown in figure 4-1.

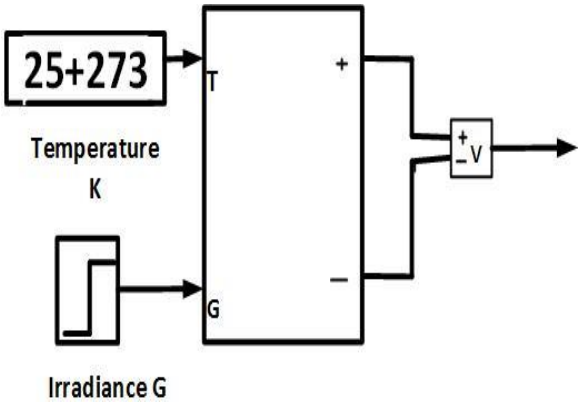

Figure 4-1: shows Simulink block of the photovoltaic array [31].

This initial set up is used to obtain I-V, P-V curve. Then same model has been used to obtain I-V and P-V curve by keeping irradiance or temperature constant. Effect on curve using both conditions has been observed. P-V model has been attached to boost as well as Single phase full bridge inverter. Best value of Rs and Rp has

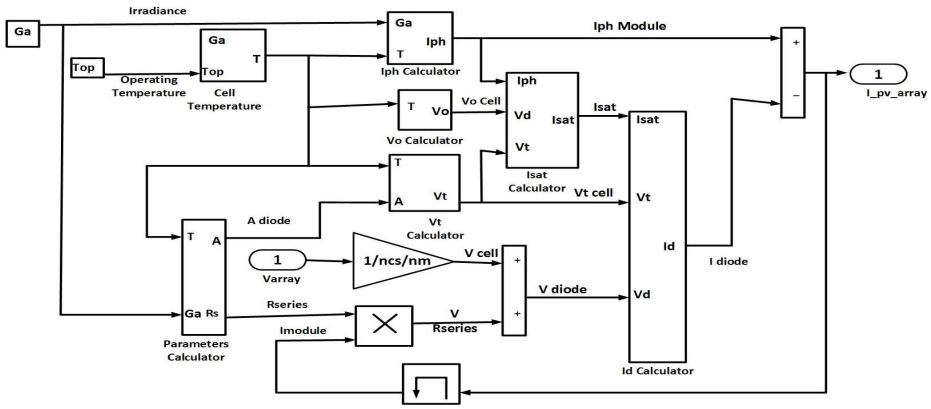

Figure 4-2: shows I-V characteristic model [9].

been calculated to get maximum power point of PV. Model of photovoltaic array has been implemented given in figure 4-2. Matlab Simulink model uses control current source. Initially specified value of irradiance and temperature has been used. Six panel in series has been used and set of six panel connected in parallel. So total 12 panel has been used. This has internal series cell around 72 per panel. In this number of series and parallel set are denoted by ns and nm. Current I used for controlled current source. Controlled current source using best value of R_s nad R_p for boost converter has been used. R_s and R_p is the intrinsic series and shunt resistance respectively. Value for R_s is very small and R_p is of very high value [3]. Irradiance and temperature has been used as input for solar array to get output voltage and current.

4.2 Simulation Model of Boost Converter with MPPT Controller

In boost converter model, output of photovoltaic array has been used as input for boost converter. Boost converter can be used as switching mode regulators to convert an unregulated dc voltage to a regulated dc output voltage. It is achieved by using PWM at fixed frequency and IGBT. To maximize efficiency, the minimum oscillator frequency should be about 100 times longer than the transistor switching time. The switching loss in the transistor is limitation. The transistor switching loss increases with the switching frequency. It decreases the efficiency as well. High frequency

operation is limited due to core loss. The PWM control signal for the dc converter is used to get required output. Initially for open loop, pulse generator has been used to control duty cycle. And in case of close loop boost converter, MPPT algorithm has been used. Figure 4-3 shows PV array boost converter with MPPT algorithm.

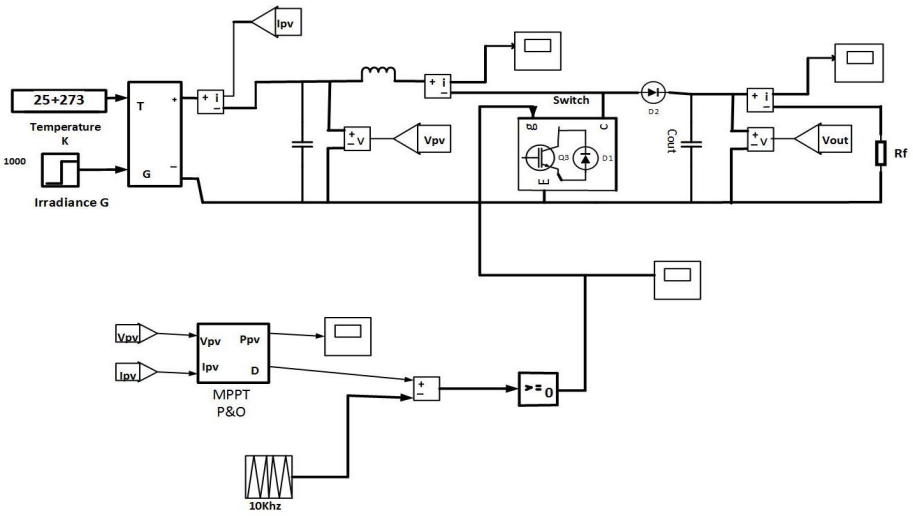

Figure 4-3: shows Simulink model of the photovoltaic system with MPPT controller & boost converter [31].

By tracking maximum power, efficiency for PV system has been increases at different environmental condition. MPPT has been used to extract the maximum power from the solar PV module and transfer that to the load. That will achieve by controlling duty cycle. In this case load impedance seen by source is varied which match point of peak power with source. MPPT is not a mechanical tracking system that physically moves panel. It is a fully electronic system that varies the electrical operating point of the modules to deliver maximum available power.

4.3 Simulation of Full Bridge and grid connected Inverter with SPWM

Initially full bridge inverter has been tested in open loop. Power at input is equal to power at output has been checked using simple pulse generator. To reduced distortion factor and lower order harmonics, width of each pulse is varied in proportion

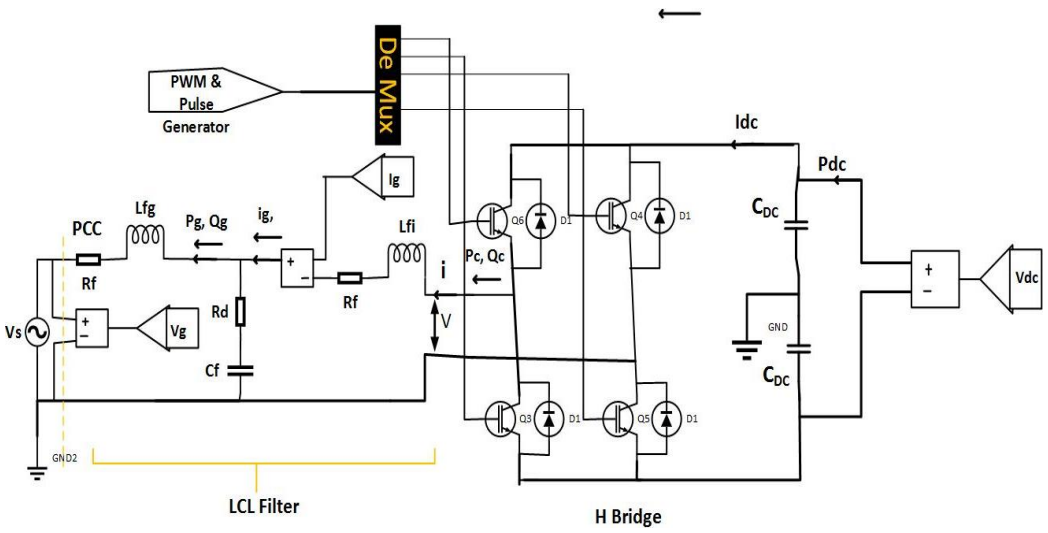

Figure 4-4: shows Simulink model of the Full Bridge VSC [31].

to the amplitude of a sine wave and is evaluated at the centre of the same pulse. The frequency of reference signal determines the inverter output frequency and its peak amplitude reference signal. Then it controls the modulation index m and V_{rms} output voltage V_o. Carrier frequency control number of pulses per half cycle. In PWM switching technique, DC input voltage is usually constant in magnitude. And produced output AC voltage where magnitude and frequency can be controlled. Frequency for trianguler wave is same as switching frequency and is kept constant.

Switching frequency of triangular wave controls speed at which the inverter switches are turned off and on. Modulation ratio m_a is used to control duty cycle of one of inverter switches. Duty cycle control based on comparison of reference ($V_{control}$) and triangular carrier signal (V_{tri}). The various frequency triangular carriers with different amplitude modulation ratio SPWM signal had been programmed and tested in single phase inverter. The two switches are never off at the same time which results to avoid output voltage fluctuation between $\pm\frac{V_{dc}}{2}$.

Because of Unipolar switching, output voltage level changes between either 0 to -V_{dc} or from 0 to +V_{dc}, this scheme has the effect of doubling the switching frequency as far as the output harmonics are concerned, compared to the bipolar switching scheme. To generate an AC waveform in single-phase inverter, the switches S1, S2 ON or S3, S4 on for respective period to get alternate positive as well as negative voltage. Two

switches in same leg should not be turn on at same time. Final sinusoidal fundamental component as shown in figure 4-5. The load voltage is calculated by

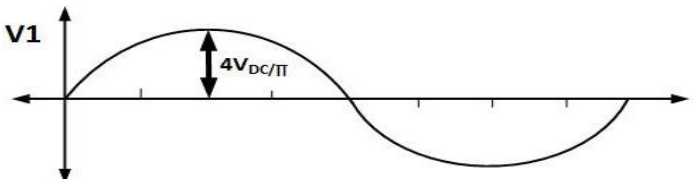

Figure 4-5: shows Fundamental Component

$V_o = V_{dc}$ For Period $0 < \Theta < \pi$

$V_o = -V_{dc}$ For Period $0 < \Theta < \pi$

The resulting output voltage has a fundamental alternating component. To avoid short circuit, blanking time (dead time) across the DC bus has been introdused. The blanking time introduces low order harmonics to the voltage of the output. That is very difficult to filter out. The n-th harmonic of the output voltage is given by Fourier analysis 4.1 [35].

$$V_n = 4 * V_{dc} \frac{\cos(n\alpha)}{n * \pi} \tag{4.1}$$

n=1,2,3....

Where

α: The blanking time along with the scale of each harmonic rests on it.

The angle α decides magnitude of the harmonic. Harmonic has been reduced by PWM technique. High frequency signal has been used to reduce number of filter. The resulting output voltage include fundamental alternating component. Voltage includes high frequency harmonics. The harmonics can be filtered with LCL filter or by implementing appropriate modulation techniques. The instantaneous inductive load current is given in 4.2 [35].

$$i_{load}(\phi) = \frac{V_{dc}}{R} - \frac{V_{dc}}{R}(1 + \tanh(\frac{\pi * R}{2 * \omega}))e^{-(\frac{\phi * R}{\omega * L})} for 0 < \phi < \pi \tag{4.2}$$

$$i_{load}(\phi) = -\frac{V_{dc}}{R} - \frac{V_{dc}}{R}(1 + \tanh(\frac{\pi * R}{2 * \omega}))e^{-(\frac{(\phi - \pi) * R}{\omega * L})} for 0 < \phi < 2\pi \tag{4.3}$$

Figure 4-6 shows complete diagram for single stage Full bridge VSC.

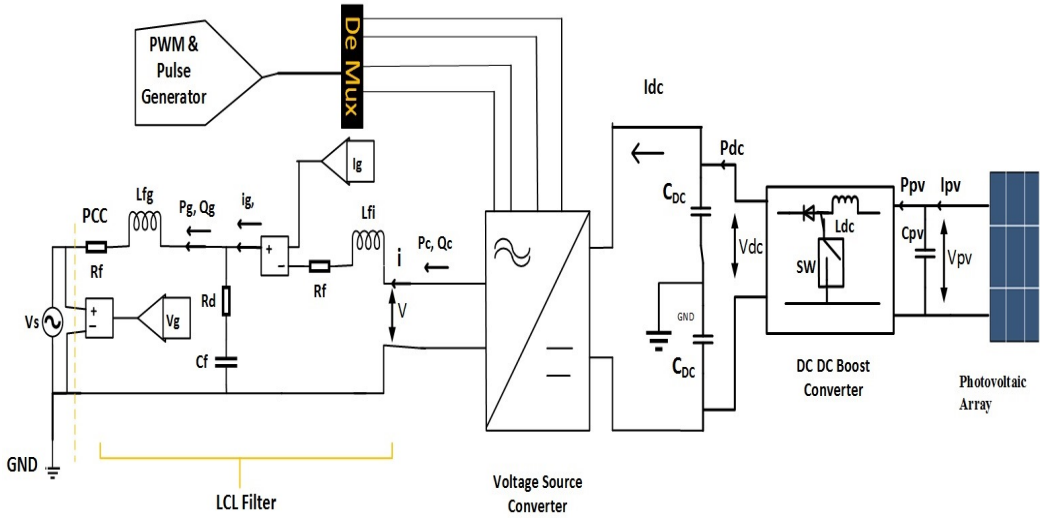

Figure 4-6: shows Simulink model Single Phase Two stage Full Bridge VSC [31].

Chapter 5

Simulation Result

5.0.1 Simulation of PV with variation in Temperature & Irradiance

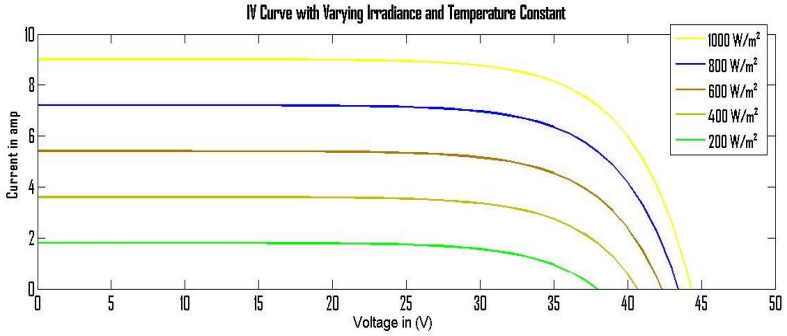

Figure 5-1: I-V characteristic of a solar array for a fixed temperature but varying irradiance [31]

The I-V & P-V curves shown in figure 5-1 & 5-2 respectively for various irradiance but a fixed temperature (25°). It has been observed that the open circuit voltage decreases with increase in irradiance at a fixed temperature. Moreover, from the I-V & P-V curves shown in figure 5-3 & 5-4 respectively at a fixed irradiance at 1000 W/m^2, it has been observed that the open circuit voltage decreases with increase in temperature. From the I-V curve shown in figure 5-1, short circuit current has been increases with increase in irradiance at a fixed temperature.

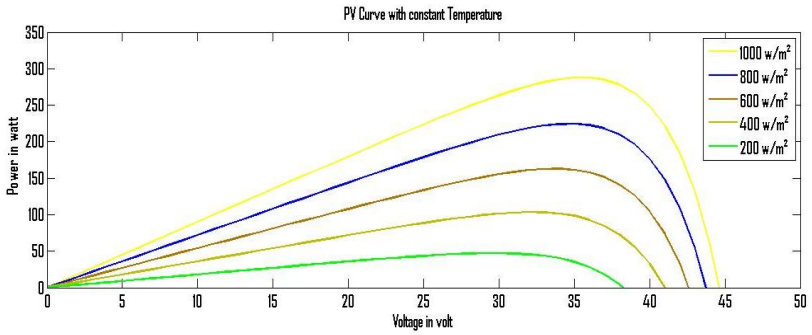

Figure 5-2: P-V characteristic of a solar array for a fixed temperature but varying irradiance [31]

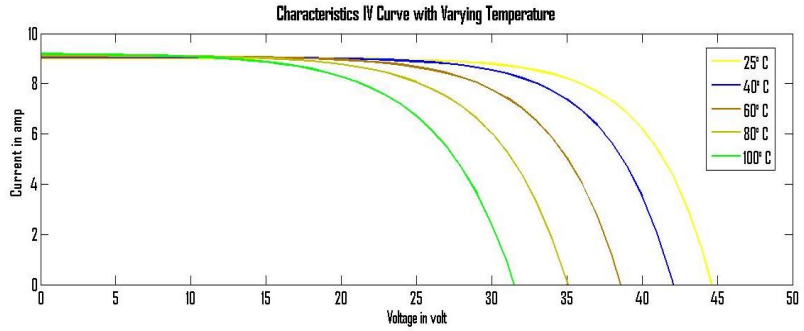

Figure 5-3: I-V Characteristic of a PV array under a fixed irradiance but varying Temperatures [31]

5.0.2 Effect of Change in Irradiance for Photovoltaic output Power, Voltage, Current, DC-link voltage & Active-Reactive Power

The simulation is run at 0.6s. At the beginning, the irradiation is set at G=1000 W/m^2 and at t=0.3 s a step change of irradiation to 600 W/m^2 is performed. The output power of the PV varies from 3.947 kW to 2.383 kW as shown in figure 5-5. Though there is a variation of the irradiance, PV array operates at maximum power.

Figure 5-6 shows step change in output voltage of PV array with respect to change in irradiance. The output voltage oscillates around the maximum power due to P&O algorithm. Figure 5-7 shows step change in output current of PV array with respect to change in irradiance. The PV array current Ipv reaches steady state after 0.002 s shown in figure 5-8. Moreover, the current oscillates around the MPP. The current

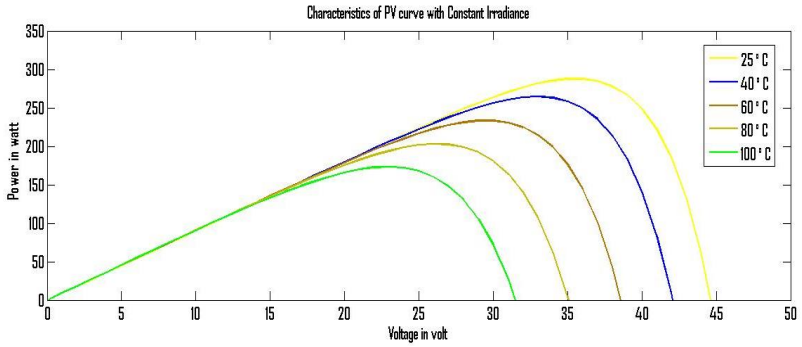

Figure 5-4: P-V Characteristic of a PV array under a fixed irradiance but varying Temperatures [31]

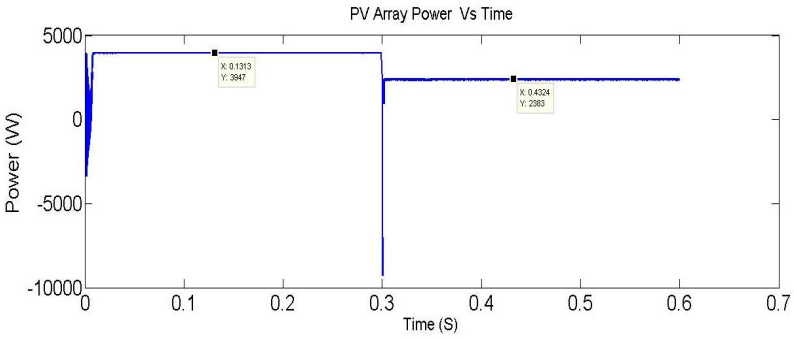

Figure 5-5: shows Step change in the Photovoltaic Power Output [31]

drops from 17.02 A to 10.41 A with respect to irradiance at 0.3s. At 600 W/m^2 irradiances, current 10.41 A which is the maximum current of the PV array. Maximum power almost track instantly by MPPT.

Figure 5-10 & 5-9 shows step change in grid voltage & current respectively of Single Phase Full Bridge Inverter with respect to change in irradiance. Figure 5-11 & 5-12 shows change in DC link voltage & Active-Reactive power respectively of Single Phase Full Bridge Inverter with respect to change in irradiance.

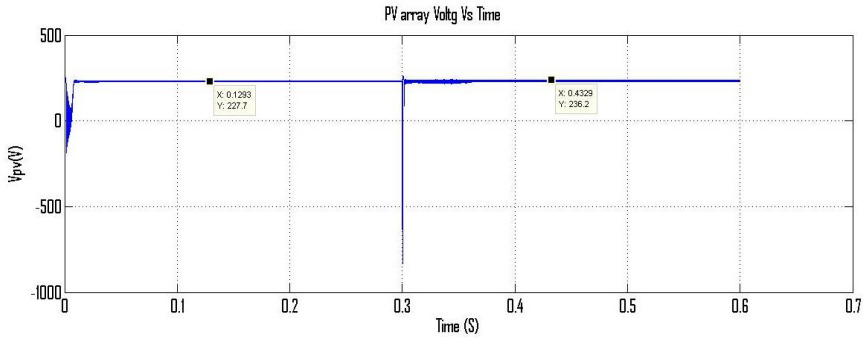

Figure 5-6: shows Step change in the Photovoltaic PV array Output Voltage [31]

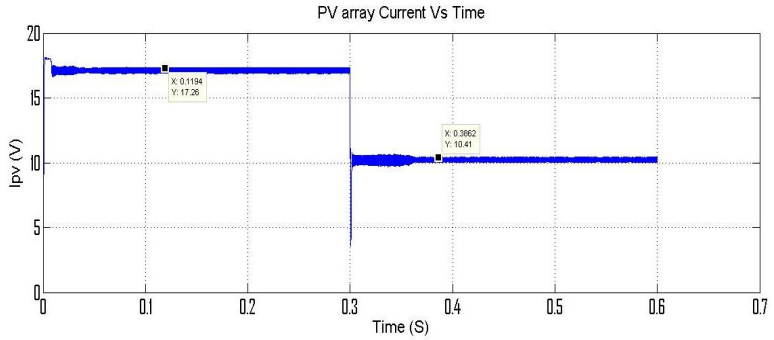

Figure 5-7: shows Step change in the Photovoltaic PV array Output Current [31]

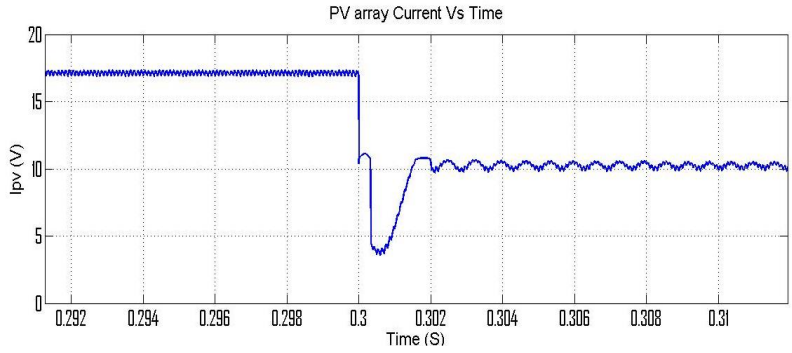

Figure 5-8: shows PV array current Ipv reaches steady state after 0.002 s [31]

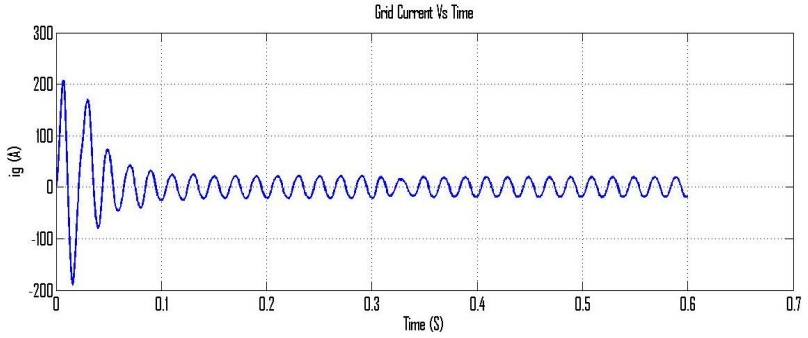

Figure 5-9: shows Step change in the Single Phase Full Bridge Inverter Grid Current [31]

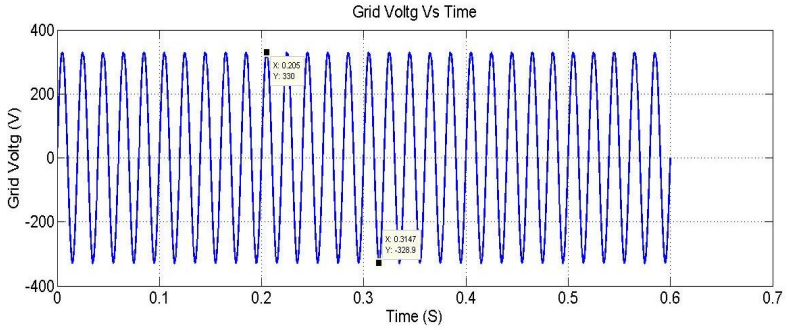

Figure 5-10: shows Step change in the Single Phase Full Bridge Inverter Grid Voltage [31]

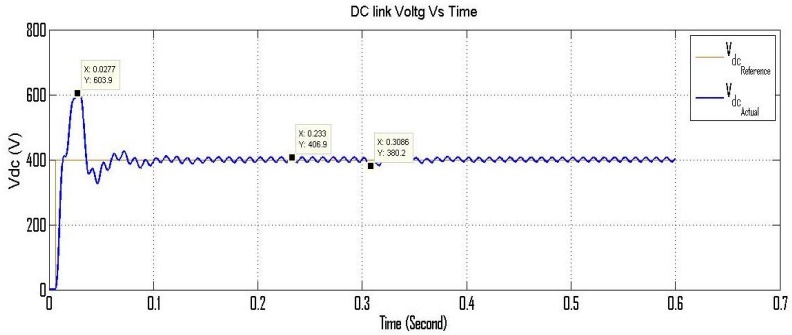

Figure 5-11: shows change in the Single Phase Full Bridge Inverter DC link Voltage [31]

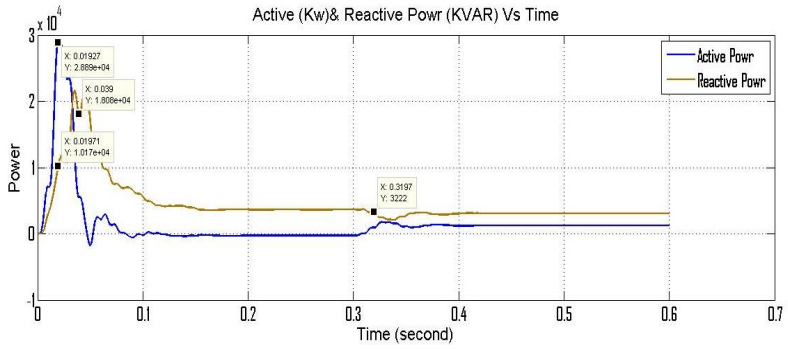

Figure 5-12: shows change in the Single Phase Full Bridge Inverter for Active-Reactive Power [31]

Chapter 6

Conclusion & Future Work

6.1 Conclusion

With help of PV & IV curve shown in simulation, characteristics for voltage, current, power has been verified and is the same as the characteristics given from the data sheet. PV models output voltage & current vary with respect to change in irradiance or temperature. Maximum power has been achieved irrespective of operation condition with help of Perturb & observe algorithm which can track maximum power point of the PV array.

Whole single phase two stage full bridge grid connected DC-DC-AC inverter with maximum point has been analysed and simulated. Finally, DC voltage generated by PV array could produce AC sinusoidal current at output of inverter. Finally, PV power decides, amplitude of current. SPWM (sinusoidal pulse width modulation) unipolar technique and designed LCL filter has been used to get grid voltage and current with less harmonics and distortion. To control DC link voltage and current, current and voltage control loop has been used.

6.2 Future work

Following are the future scope of work:

* Extensive simulation of the Single phase two stage grid connected photovoltaic

system should be done. To keep the boost converter output voltage constant, Perturb and observation MPPT controller has been used. The fast-inner current loop with a slower outer voltage loop are designed with help of LCL filter to eliminate harmonic. For further improvement, this method can be used.

∗ Single phase grid connected system can be used as a basic guideline when designing the grid connected PV inverters and their controls 50Hz and 240V point of common coupling (PCC) voltage.

∗ With better control on active and reactive power, research on power management can also be conducted for future work.

∗ More advance voltage control techniques and operating and coordination strategies developed with help of Thesis can be evaluated by carrying out simulation studies on PV systems integrated to three-phase four wire systems and to Distributed resources (DR) for further development.

∗ When PV system is integrated with a battery storage system, power curtailing may not be necessary in certain situations. In future, it is beneficial to integrate developed PV system with a battery storage systems.

Appendix A

A.1 Boost Converter

A.1.1 Selection of Inductor

The inductor determines the stability of the current sensor loop and the inductor current ripple. The peak-to-peak inductor ripple current is inversely proportional to the inductor value. There are two ways to calculate current ripple. To calculate inductor, ΔI_L has been assumed to 5 % of the rated input current of the DC-DC boost converter.

Assumed ΔI_L=0.51 for Best Result

Then L_{dc} has been calculated using below formula:

$$L_{DC} = \frac{V_{pv}(V_{dcavg} - V_{pv})}{\Delta I_L f_{dc} V_{dcavg}} \tag{A.1}$$

$V_{dcavg} = 400V$ Average DC-link voltage and

$f_{dc} = 10KHz$ Switching frequency of the DC-DC boost converter.

$V_{pv} = 215$ V Input voltage to the DC-DC boost converter i.e. PV array voltage.

$\Delta I_L = 0.51$ Current ripple

Here PV system is operated at the rated capacity. Further, the rated capacity of the DC-DC boost converter is 5 KW.

Calculated value of $L_{dc} = 19.49$ mH using equation A.1.

Best Selected value $L_{dc} = 19$ mH

A.1.2 Selection of Input Capacitor

Decoupling of the PV array or DC from AC side dynamics accomplished due implemented control techniques nor due to large capacitor. Large value of capacitor allows PV array to be decoupled from AC side. The capacitor C_{pv} was mainly utilised to minimise the switching frequency ripple current that is drawn from the PV array and switching frequency ripple voltage as well. That why smaller value of capacitor has been used. Equation has been used to calculate C_{pv}.

$$C_{pv} = \frac{V_{pv}D}{4 * \Delta V_{pv} f_{dc}^2 L_{dc}} \tag{A.2}$$

$D = 1 - \frac{215}{400} = 0.4625$ Duty cycle of the DC-DC boost converter,
$V_{pv} = 215$ V Average voltage across the PV array,
ΔV_{pv}=20 V Assume Switching ripple voltage of the PV array,
L_{dc}=$19 * 10^{-3}$H
f_{dc}=10 kHz.
Calculated C_{pv}=0.621 μF implemented in PV system in order to limit ΔV_{pv}.
Selected Best Value C_{pv}=0.584 μF

A.1.3 Selection of output Capacitor

Equation A.3 has been used for selection of boost converter output capacitor. It depends on minimum ripple voltage. This output capacitor acts as DC link capacitor.

Since,

$P_{in} = 215 * 17.02 = 3659.3W = P_{out}$
$I_{out} = \frac{P_{out}}{V_{out}} = \frac{3659.3}{400} = 9.14825$ A
$R_{load} = \frac{V_{load}}{I_{out}} = \frac{400}{9.14825} = 44$ Ohm

$$C_{DC} = \frac{V_{load}D}{f_s R_{load} \Delta V_{load}} = \frac{400 * 0.46}{10 * 10^3 * 44 * 20} = 21.02\mu F \tag{A.3}$$

C_{DC} has been selected of higher value. So $C_{DC} = 2.5mF$

where V_{load}: output voltage of the boost converter

ΔV_{load}: output ripple voltage

Due to variation in temperature and irradiance, output voltage of PV array also varies. DC link capacitor is installed between the PV and the inverter to compensate the variation of the output voltage of the PV. Proper selection of DC link capacitor reduces voltage ripple and offer energy storage for short period of time.

Appendix B

B.1 LCL Filter

In LCL filter includes two inductors and capacitor connected in parallel i.e. per phase. In above LCL filter R_f and L_g are grid side resistor and Inductor respectively. And R_i and L_i is inverter side inductor. In this C_f is parallel capacitor and R_d is resistor for passive damping [15].

B.1.1 Basic Equation

The voltage at the output of the VSC, the voltage across C_f and R_d and the grid voltage are v, v_c and v_g respectively. The output current of the VSC and the current injected to the grid by the VSC are i and i_g respectively. The grid voltage appears as a short circuit for all the harmonic voltages created by the VSC as grid voltage. It is assumed as a pure sinusoid at fundamental frequency, $'f'$. The harmonic number is denoted by "$\backslash nh''$.

$$G_{LCL}(s) = \frac{(i_g(s))}{v(s)} = \frac{R_d * C_f s + 1}{As^3 + Bs^2 + Cs + D} \tag{B.1}$$

Where A $= L_{fc} * L_{fg} * C_f$

B$= (L_{fc}R_{fg} + L_{fg}R_{fc} + (L_{fc} + L_{fg}) * R_d) * C_f$

C $= (R_{fg}R_{fc} + R_{fc}R_d + R_{fg}R_d)C_f + L_{fc} + L_{fg}$

D $= R_{fc} + R_{fg}$

After neglecting resistance of each inductor,

$G_{LCL}(s) = \frac{(i_g(s))}{v(s)}$

$$G_{LCL}(s) = \frac{R_d * C_f s + 1}{s(L_{fc} * L_{fg} * C_f s^2 + (L_{fc} + L_{fg}) * R_d * C_f s + L_{fc} + L_{fg})} \tag{B.2}$$

Further, if damping resistance is neglected;

$$G_{LCL}(s) = \frac{i_g(s)}{v(s)} = \frac{1}{s(L_{fc} * L_{fg} * C_f s^2 + L_{fc} + L_{fg})} \tag{B.3}$$

Equation B.3 can be presented as follows,

$$\frac{i_g(s)}{v(s)} = \frac{1}{s(L_{fc} * L_{fg} * C_f s^2 + L_{fc} + L_{fg})} \tag{B.4}$$

Where

$Z_{LC}^2 = \frac{1}{L_{fg} * C_f}$

and

$\omega_{res}^2 = \frac{L_{fc} + L_{fg}}{L_{fc} * L_{fg} * C_f}$

LCL filter has been designed to reduce switching ripple in grid current. In below procedure, relationship between the converter side current and voltage has been derived. There are two ways to design LCL filter any frequency. In first, assume filter capacitance should be with very small impedance. Capacitor acts as short circuit as frequency is higher than switching frequency of VSC, f_{sw}.

$$\frac{i(s)}{v(s)} = \frac{1}{sL_{fc}} \tag{B.5}$$

From equation B.3 and B.4;

$$\frac{i_g(s)}{i(s)} = \frac{Z_{LC}^2}{S^2 + \omega_{res}^2} \tag{B.6}$$

In other way, it has been derived in equation B.6. Grid voltage considered as short

Table B.1: Specifications of the VSC

Parameter	Value
P_r	5.4 KW
V_r	230
V_{dc}	400
f	50 Hz
f_{sw}	25 KHz

circuit for harmonics. So, frequency is higher than switching frequency of VSC, f_{sw}.

$$\frac{i_g(s)}{i(s)} = \frac{Z_{LC}^2}{S^2 + Z_{LC}^2} \tag{B.7}$$

It has been proved while analysing the performance of a designed LCL filter. Defining base quantities for the VSC system.

$$Z_b = \frac{V_r^2}{P_r^2} \tag{B.8}$$

$$C_b = \frac{1}{\omega * Z_b} \tag{B.9}$$

Detail design procedure & constraints of LCL Filter explained in reference [24] [23] [13] [2] [30].

B.1.2 Designing Procedure for 5 kVA Single-Phase VSC

Base values can be calculated as $Z_b = 9.8$ and $C_b = 325$ F by using B.8 and B.9 respectively. The peak switching ripple current, Δi_p through L_{fc} to a given value can be obtained from B.10 [14] [10] to limit L_{fc} inductance. VSC has been modulated with sinusoidal unipolar PWM and with the modulation index, 'm' is $0.5 < m < 1$. Then only equation B.10 will be valid.

$$L_{fc} = \frac{V_{dc}}{16 * f_{sw} \Delta i_p} \tag{B.10}$$

L_{fc} can be calculated as 300 μH using B.10. Switching ripple current attenuated to 10 % of the rated peak current of the VSC i.e. 10%*33=3.3 A.

Table B.2: LCL designed Filter Parameters

Parameter	Value
L_{fc}	3 mH
L_{fg}	1.5 mH
C_f	$2.6\mu F$
R_d	1.5 ohm
f	50 Hz
f_{sw}	25 KHz

$C_f < 16.25\mu F$ as per constraint 1 given in Section [30]. Change of $'r'$ is not significant when $C_f > 2\mu F$, detail explanation gven in [30]. Though capacitance of C_f increased beyond $2\mu F$, there will not be much reduction in the size of L_{fg}. So, the Selected $C_f = 2.6\mu F$ for designing the filter, to calculate value r. $L_{fg} = 150\mu H$ [30].

The resonant frequency of the LCL filter, f_{ref} is 10 kHz. The total inductance of the LCL filter is 0.015 pu, if $L_{fc} = 300\mu H$ and $L_{fg} = 150\mu H$ and $C_f = 2\mu F$. This is how constraints 2 and 3 are satisfied explained in [30]. R_d damping resistor is chosen as one third of the impedance of the filter capacitor at 25 kHz. LCL designed filter parameters for best result are given in table B.2. In detailed design for LCL filter has been explain in [30] [15].

Appendix C

C.0.1 Selection DC-link Capacitor

Stored energy in Capacitor is given by below equation.

$$\Delta e(t) = \frac{P}{2 * \omega} * Sin(2\omega t) \tag{C.1}$$

The difference in the maximum and the minimum energy stored in C_{dc}, Δe_{max} that is the energy difference when $(2\omega t)=\frac{\pi}{2}$ and $(2\omega t)= -\frac{\pi}{2}$ is given by

$$\Delta e_{max} = \frac{P}{\omega} \tag{C.2}$$

The maximum and the minimum energy stored in C_{dc} causes the maximum and the minimum voltages at C_{dc} since the voltage across a capacitor is proportional to the stored energy in the capacitor. Therefore Δe_{max} can be written in terms of the maximum and the minimum DC-link voltages that are V_{dcmin} and V_{dcmax} respectively as given in

$$\Delta e_{max} = \frac{1}{2} * C_{dc} * (V_{dcmax}^2 - V_{dcmin}^2) \tag{C.3}$$

An expression for the peak-peak 100 Hz DC-link voltage ripple, ΔV_{dc}, can be derived as given in (C.6) from (C.2) and (C.3). Equation (C.5), is the average DC-link voltage of the VSC.

$$\Delta V_{dc} = V_{dcmax} - V_{dcmin} \tag{C.4}$$

$$V_{dcavg} = \frac{(V_{dcmax} + V_{dcmin})}{2} \tag{C.5}$$

$$\Delta V_{dc} = \frac{P}{(C_{dc} * V_{dc} * \omega)} \tag{C.6}$$

The capacitor at the DC-link should be large to reduce the DC-link voltage ripple almost to zero as per (C.6). Practically it is not possible and there is a limitation to the size of C_{dc}. But voltage ripple at DClink voltage of a single-phase VSC has been controlled. The ΔV_{dc} is 5 % of V_{dcavg} i.e. 20 V. With reference to value given in table B.1, C_{dc} calculated 2.2 mF. C_{dc} selected best value 2.5 mF. Detailed design procedure for DC-link capacitor has been explained in [30] [42] [16] [20] [33].

Appendix D

D.1 Data Sheet SLK72M6L

Figure D-1: shows Data Sheet SLK72M6L. [19].

SLK72M6L 285 Wp - 310 Wp

Módulos solares monocristalinos

siliken

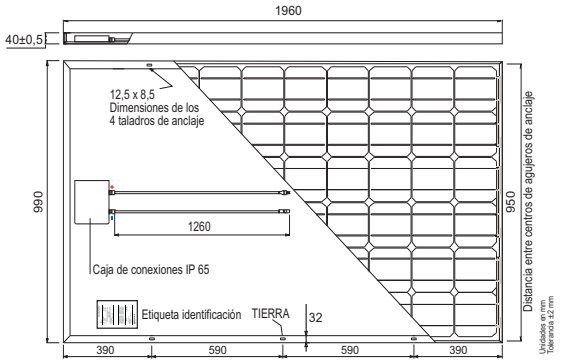

Características constructivas

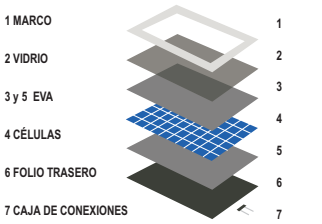

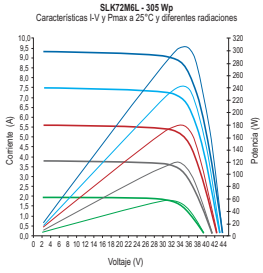

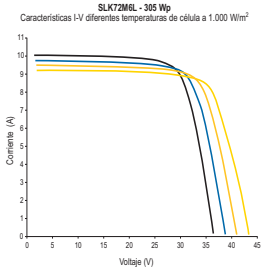

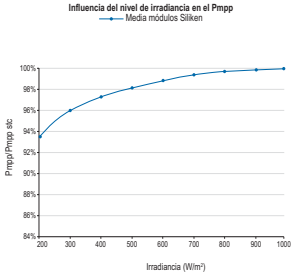

Datos mecánicos

Dimensiones (LxAxF)	1960 x 990 x 40 mm
Peso	23 kg
Cables de salida	Longitudes de cable simétricas de 1,26m, Ø4 mm², doble capa aislante, libre de halógenuros, resistente a la radiación UV
Caja de conexiones	IP-65 con diodos bypass de protección
Marco	Aleación de aluminio anodizado de 15 micras de espesor tipo 6063 T6
Vidrio delantero	Vidrio templado de 3,2 mm con bajo contenido de hierro con elevada capacidad de transmisión
Células solares	72 células monocristalinas 156 x 156 mm

Datos eléctricos

Potencia máxima a STC (+3/0 %)	P_{mp} (Wp)	285	290	295	300	305*	310*
Eficiencia a STC	η (%)	14,7	14,9	15,2	15,5	15,7	16,0
Factor de llenado	FF	0,761	0,759	0,759	0,758	0,76	0,763
Voltaje a potencia máxima	V_{mp} (V)	35,7	35,7	35,7	35,8	35,8	35,9
Corriente a potencia máxima	I_{mp} (A)	7,98	8,12	8,25	8,38	8,51	8,63
Voltaje de circuito abierto	V_{oc} (V)	44,2	44,4	44,4	44,4	44,5	44,5
Voltaje de cortocircuito	I_{sc} (A)	8,47	8,61	8,75	8,91	9,02	9,13
Voltaje máximo UL / IEC	V_{max} (V) UL/IEC	600 / 1000					
Coeficiente temperatura de Pmp	T_kP_{mp} (%/ºC)	-0,41					
Coeficiente temperatura de Voc	T_kV_{oc} (%/ºC)	-0,360					
Coeficiente temperatura de Isc	T_kI_{sc} (%/ºC)	+0,06					
Temperatura de célula normal de operación	NOCT (ºC)	47±2					
Fusibles de protección	A	11					
Diodos By-pass	A/V	12/40					
Ensayo de corriente inversa	A	13,5					

Datos referidos a condiciones estándar de ensayo STC: Radiación de 1.000 W/m², con espectro AM 1.5 y temperatura de célula de 25ºC
*Sujeto a disponibilidad.

Certificados

Registrado en UL e Intertek	UL ORD-C1703-01 / UL1703
Categoría ignífuga	Clase C
Certificación TÜV	IEC 61215 / IEC 61730 / 61701 ensayo niebla salina
ISO 9001:2000	Nº ES08/5170
ISO 14001	Nº ES09/6520
Declaración de conformidad CE (marca CE)	

Condiciones de operación comprobadas

Temperatura	-40 ºC a +85 ºC
Carga estática	2400 Pa
Carga máxima	5400 Pa
Resistencia al impacto	Impacto por granizo Ø25 mm a 23 m/s

Garantía de producto

10 años de garantía en materiales y mano de obra

25 años de garantía de potencia lineal

Primer año: 97% de la potencia etiquetada

Del año 2 al 25: reducción máxima de potencia de 0,7% p.a.

siliken manufacturing
C/ Massamagrell, 13 • Pol. Ind L'Horteta.
46138 Rafelbunyol - Valencia - España

ADVERTENCIA: Lea atentamente el manual de instrucciones antes de utilizar el producto
NOTA: Siliken Manufacturing, S.L.U. se reserva el derecho a modificar este producto sin notificarlo

Junio 2011

Siliken S.A. · Ronda Isaac Peral y Caballero, 14 · 46980 Paterna - Valencia - **España** · Tel.: (+34) 902 41 22 33 · Fax: (+34) 96 070 92 65 · info@siliken.com · www.siliken.com

Figure D-2: shows Data Sheet SLK72M6L. [19].

Bibliography

[1] L[eslie] A. Aamport. The gnats and gnus document preparation system. *G-Animal's Journal*, 41(7):73+, July 1986. This is a full ARTICLE entry.

[2] C. Bao. Step-by-step controller design for lcl-type grid connected inverter with capacitor current-feedback active-damping. *IEEE Trans. Power Electron*, 29(3):1239, March 2014.

[3] Habbati Bellia, Ramdani Youcef, and Moulay Fatima. A detailed modeling of photovoltaic module using matlab. *NRIAG Journal of Astronomy and Geophysics*, 3(1):53–61, 2014.

[4] Sergio Augusto Oliveira da Silva, Leonardo Bruno Garcia Campanhol, Alessandro Goedtel, Claudionor F Nascimento, and Denilson Paiao. A comparative analysis of p-pll algorithms for single-phase utility connected systems. In *Power Electronics and Applications, 2009. EPE'09. 13th European Conference on*, pages 1–10. IEEE, 2009.

[5] Debashis Das. *Modeling and simulation of PV array with boost converter: An open loop study*. PhD thesis, NATIONAL INSTITUTE OF TECHNOLOGY ROURKELA, 2011.

[6] Sairaj V Dhople, Ali Davoudi, and Patrick L Chapman. Dual-stage converter to improve transfer efficiency and maximum power point tracking feasibility in photovoltaic energy-conversion systems. In *Applied Power Electronics Conference and Exposition (APEC), 2010 Twenty-Fifth Annual IEEE*, pages 2138–2142. IEEE, 2010.

[7] JHR Enslin and PJM Heskes. Harmonic interaction between a large number of distributed power inverters and the distribution network. In *Power Electronics Specialist Conference, 2003. PESC'03. 2003 IEEE 34th Annual*, volume 4, pages 1742–1747. IEEE, 2003.

[8] Trishan Esram and Patrick L Chapman. Comparison of photovoltaic array maximum power point tracking techniques. *IEEE Transactions on energy conversion*, 22(2):439–449, 2007.

[9] Cristina Gonzalez-Moran, P Arboleya, G Diaz, and J Gomez-Aleixandre. Modeling photovoltaic dc primary sources as grid connected inverter supplies considering non linear effects. In *Electrical Power Conference, 2007. EPC 2007. IEEE Canada*, pages 50–55. IEEE, 2007.

[10] D Grahame Holmes and Thomas A Lipo. *Pulse width modulation for power converters: principles and practice*, volume 18. John Wiley & Sons, 2003.

[11] KH Hussein, I Muta, T Hoshino, and M1 Osakada. Maximum photovoltaic power tracking: an algorithm for rapidly changing atmospheric conditions. *IEE Proceedings-Generation, Transmission and Distribution*, 142(1):59–64, 1995.

[12] Baharuddin Ismail. *Design And Development Of Unipolar SPWM Switching Pulses For Single Phase Full Bridge Inverter Application [TK7871. 85. B151 2008 f rb].* PhD thesis, Universiti Sains Malaysia, 2008.

[13] S. Hansen J. Dannehl, F. Fuchs and P. Thgersen. Investigation of active damping approaches for pi-based current control of grid-connected pulse width modulation converters with lcl filters. *IEEE Trans. Ind. Appl.*, 46(4):1509, August 2010.

[14] F Jenni and D Wüest. Steuerverfahren für selbstgeführte stromrichter (switching method for self-commutated converter). *Hochschulverlag AG an der ETH Zürich, BG Tubner Stuttgart, Germany*, 1995.

[15] Hea-Gwang Jeong, Kyo-Beum Lee, Sewan Choi, and Woojin Choi. Performance improvement of lcl-filter-based grid-connected inverters using pqr power transformation. *IEEE Transactions on Power Electronics*, 25(5):1320–1330, 2010.

[16] CENGİZ KAHRAMAN, BAŞAR ÖZTAYŞI, and SEZI CEVIK ONAR. Photovoltaics type selection using a projection model-based approach to intuitionistic fuzzy multicriteria decision making. In *Uncertainty Modelling in Knowledge Engineering and Decision Making: Proceedings of the 12th International FLINS Conference*, pages 924–929. World Scientific, 2016.

[17] Tamás Kerekes, Remus Teodorescu, Pedro Rodríguez, Gerardo Vázquez, and Emiliano Aldabas. A new high-efficiency single-phase transformerless pv inverter topology. *IEEE Transactions on Industrial Electronics*, 58(1):184–191, 2011.

[18] David L King, Jay A Kratochvil, and William Earl Boyson. *Photovoltaic array performance model*. United States. Department of Energy, 2004.

[19] Soeren Baekhoej Kjaer, John K Pedersen, and Frede Blaabjerg. A review of single-phase grid-connected inverters for photovoltaic modules. *IEEE transactions on industry applications*, 41(5):1292–1306, 2005.

[20] David Leuenberger and Jürgen Biela. Pv-module-integrated ac inverters (ac modules) with subpanel mpp tracking. *IEEE Transactions on Power Electronics*, 32(8):6105–6118, 2017.

[21] Marco Liserre, Antonio Dell'Aquila, and Frede Blaabjerg. Stability improvements of an lcl-filter based three-phase active rectifier. In *Power Electronics Specialists Conference, 2002. pesc 02. 2002 IEEE 33rd Annual*, volume 3, pages 1195–1201. IEEE, 2002.

[22] Fangrui Liu, Yong Kang, Yu Zhang, and Shanxu Duan. Comparison of p&o and hill climbing mppt methods for grid-connected pv converter. In *Industrial Electronics and Applications, 2008. ICIEA 2008. 3rd IEEE Conference on*, pages 804–807. IEEE, 2008.

[23] W. Xiao M. Hanif, V. Khadkikar and J. Kirtley. Two degrees of freedom active damping technique for an lcl filter based grid connected pv systems. *IEEE Trans. Ind. Electron.*, 16(6):2795, July 2013.

[24] F. Blaabjerg M. Liserre and Steffan Hansen. Design and control of an lcl-filter based three-phase active rectifier. *Int. J. Electron.*

[25] Sachin Maheshri and Prabodh Khampariya. Simulation of single phase spwm (unipolar) inverter. *International Journal of Innovative Research in Advanced Engineering (IJIRAE)*, 1(3), 2014.

[26] Yousef A Mahmoud, Weidong Xiao, and Hatem H Zeineldin. A parameterization approach for enhancing pv model accuracy. *IEEE Transactions on Industrial Electronics*, 60(12):5708–5716, 2013.

[27] K Manohar and P Sobha Rani. Mppt and simulation for a grid-connected photovoltaic system and fault analysis. *The International Journal of Engineering And Science (IJES)*, 1(2):158–166, 2012.

[28] Ned Mohan and Tore M Undeland. *Power electronics: converters, applications, and design*. John Wiley & Sons, 2007.

[29] Anuja Namboodiri and Harshal S Wani. Unipolar and bipolar pwm inverter. *International Journal for Innovative Research in Science & Technology*, 1(7):237–243, 2014.

[30] Brian K Perera. Modelling of inverter interfaced renewable energy resources to investigate grid interactions. 2015.

[31] Falinirina F Rakotomananandro. *Study of photovoltaic system*. PhD thesis, The Ohio State University, 2011.

[32] Dr Zainal Salam. Power electronics and drives (version 2). *Pdfheart. com*, 2002.

[33] Fritz Schimpf and Lars Norum. Parallel power decoupling for single-phase pv-inverters–making film capacitors applicable.

[34] Dezso Sera, Remus Teodorescu, and Pedro Rodriguez. Pv panel model based on datasheet values. In *Industrial Electronics, 2007. ISIE 2007. IEEE International Symposium on*, pages 2392–2396. IEEE, 2007.

[35] R Shaffer. Power electronic harmonic nalysis and fundamentals of power electronics with matlab, power quality in electrical systems. *Da vinci engineering series, Thomson learnin Inc, USA*, 2007.

[36] Jasim Farhood Sultani. Modelling, design and implementation of dq control in single-phase grid-connected inverters for photovoltaic systems used in domestic dwellings. 2013.

[37] Silvano Vergura. A complete and simplified datasheet-based model of pv cells in variable environmental conditions for circuit simulation. *Energies*, 9(5):326, 2016.

[38] http://www.coloradosolarpower.net/images/brochures/p100094/SLK60P6L

[39] https://autosolar.es/pdf/Ingeteam-Ingecon-Sun-Lite.pdf.

[40] Davood Yazdani, Majid Pahlevaninezhad, and A Bakhshai. Single-phase grid-synchronization algorithms for converter interfaced distributed generation systems. In *Electrical and Computer Engineering, 2009. CCECE'09. Canadian Conference on*, pages 127–131. IEEE, 2009.

[41] Richard Zhang, Mark Cardinal, Paul Szczesny, and Mark Dame. A grid simulator with control of single-phase power converters in dq rotating frame. In *Power Electronics Specialists Conference, 2002. pesc 02. 2002 IEEE 33rd Annual*, volume 3, pages 1431–1436. IEEE, 2002.

[42] Xiangdong Zong. *A single phase grid connected DC/AC inverter with reactive power control for residential PV application*. PhD thesis, University of Toronto, 2011.

[43] Xiangdong Zong and Peter W Lehn. Reactive power control of single phase grid tied voltage sourced inverters for residential pv application. In *IECON 2012-38th Annual Conference on IEEE Industrial Electronics Society*, pages 696–701. IEEE, 2012.